

On the phenomenology of a Z' coupling only to third-family fermions

A.A. Andrianov^a, P. Osland^{b,c}, A.A. Pankov^{c,d},
N.V. Romanenko^e and J. Sirkka^f

^a Department of Theoretical Physics, St.-Petersburg State University,
198904 St.-Petersburg, Russia

^b Department of Physics, University of Bergen,
Allégaten 55, N-5007 Bergen, Norway

^c Theoretical Physics Division, CERN, CH 1211 Geneva 23, Switzerland

^d Gomel Polytechnical Institute, Gomel, 246746 Belarus

^e Petersburg Nuclear Physics Institute, Gatchina,
Leningrad district, 188350, Russia

^f Department of Physics, University of Turku, FIN-20500 Turku, Finland

Abstract

The phenomenology of an additional $U(1)$ neutral gauge boson Z' coupled to the third family of fermions is discussed. One might expect such a particle to contribute to processes where taus, b and t quarks are produced. Precision data from LEP1 put severe constraints on the mixing and heavy-boson mass. We find that the effects of such a particle could not be observed at hadronic colliders, be it at the Tevatron or the LHC, because of the QCD background. At LEP2 and future e^+e^- linear colliders, one could instead hope to observe such effects, in particular for $b\bar{b}$ final states.

1 Introduction

We study phenomenological implications of the breaking of universality in weak interactions. Particular attention is paid to the signatures of new heavy elementary vector particles (Z' bosons), which can be detected at the present or future high-energy e^+e^- and hadron colliders. As the quarks of the third family (t and b) are significantly heavier than those of the other two families, one may speculate that such a boson may be involved in the formation of this difference, and thereby interact directly with the t and b quarks (as well as the τ and ν_τ) and only much more weakly with the lighter quarks and leptons, solely due to radiatively-created mixings.

Both the phenomenology of Z' -boson production and theoretical models for its dynamics are considered. A theoretical extension of the Standard Model adopting a new heavy Z' boson may need to include more unknown heavy fermions and scalar Higgs bosons. Otherwise the quantum anomalies break the unitarity and the mass pattern for heavy fermions will violate experimental bounds on deviations from the Standard Model in the low energy data.

There can be a variety of possible models depending on the strength of the vector and axial-vector couplings of the Z' to quarks and leptons. Additional bosons naturally appear in Grand Unification Theories [1, 2]. The left-right-symmetric model also contains at least one Z' boson [3].

Usually these Z' bosons interact universally with the fermions of all families; the phenomenology of such particles was considered by several authors [1, 2, 4, 5]. There exists a scheme in which Grand Unification symmetry breaking leads to the formation of a so-called ‘leptophobic’ and ‘hadrophilic’ Z' boson, which interacts only with hadrons. The phenomenology of such bosons was also considered [2, 6, 7]. A related idea has been advanced by Okun and collaborators, who consider a ‘leptonic’ photon [8].

A scheme with the breaking of universality in weak interactions has been studied by Dyatlov [9] in connection with the problem of the fermion mass hierarchy. It was shown that a neutral gauge boson interacting differently with the heaviest fermions naturally leads to a realistic mass hierarchy and Kobayashi-Maskawa mixing matrix. The phenomenology of a Z' interacting only with the quarks of the third family was considered recently by Holdom [10], by Frampton, Wise and Wright [11], and by Muller and Nandi [12].

Irrespective of the scheme of the Z' -boson embedding into an extended electroweak theory one should know the feasibility of detecting such a particle at a particular accelerator. Various high-energy colliders have been examined for that purpose: hadronic colliders (Tevatron and the LHC), LEP2 and future electron-positron colliders (NLC).

For $p\bar{p}$ and pp colliders the main production mechanisms are the following: $b\bar{b}$ -quark annihilation (from the small sea contribution in protons) near the Z' peak, quark-antiquark annihilation into a Z with conversion of the Z into a Z'

due to the small mixing and also gluon–gluon fusion. The Z' boson is assumed to be detected through an excess of $b\bar{b}$ or $t\bar{t}$ hadronic jets. Other processes are suppressed by the kinematics and due to small coupling constants. Numerical estimates have been made to determine whether the Z' signal can compete with the two-jet background originating from non-resonant processes. The conclusion is that the direct observation of a heavy Z' (heavier than the Z) with moderate coupling constants to b and t quarks is impossible at the $p\bar{p}$ Tevatron collider and unlikely even at the LHC.

The most interesting possibility is to investigate the feasibility of a Z' discovery at LEP2 [13] and the next generation of e^+e^- colliders whose design is now intensively discussed [14]. For these colliders the background of $\tau^+\tau^-$ and two ($b\bar{b}$ or $t\bar{t}$) jets is significantly lower than for the previous types of colliders; therefore there is a possibility of having kinematical windows for detecting a Z' boson.

The paper is organized as follows: In Sect. 2 we set up the notation and discuss constraints on the Z' from electroweak precision data. In Sect. 3 we consider production at hadronic colliders, and in Sect. 4 we consider e^+e^- colliders. Section 5 contains a brief summary. In Appendix A we discuss the constraints on the (expanded) scalar sector due to anomaly cancellations, and in Appendix B we give some formulas on the QCD background.

2 Model parameters and experimental input

We consider a model with an additional massive neutral $U(1)$ gauge boson Z' . The Lagrangian can be written in the form:

$$\mathcal{L} = \mathcal{L}_{\text{SM}} + \mathcal{L}_{Z'}$$

where \mathcal{L}_{SM} is the full Lagrangian of the Standard Model (SM) and $\mathcal{L}_{Z'}$ is an additional term:

$$\mathcal{L}_{Z'} = \mathcal{L}_{\text{YM}} + \mathcal{L}_{\text{Higgs}} + \mathcal{L}_{\text{int}}.$$

Here \mathcal{L}_{YM} is the usual free Yang–Mills Lagrangian for the Z' boson, $\mathcal{L}_{\text{Higgs}}$ the Lagrangian for scalar particles interacting with the Z' (one may consider different choices for the Higgs sector—some possible Higgs structures are discussed in Appendix A—see also [11, 15]), and \mathcal{L}_{int} specifies the interactions of the additional neutral boson with fermions.

2.1 Additional NC interactions

We assume that the Z' interacts only with fermions of the third family. Then the neutral-current Lagrangian is of the form [2]:

$$-\mathcal{L}_{\text{NC}} = eJ_{\text{em}}^\mu A_\mu + g_Z J^\mu Z_\mu + g_{Z'} J'^\mu Z'_\mu, \quad (2.1)$$

where the first two terms are just those of the SM and J'^μ involves only the third-family fermions, t , b , τ and ν_τ . This form of \mathcal{L}_{NC} corresponds to the case where the new $U(1)$ neutral gauge particle is not mixed with the photon [15].

In the usual notation of the SM one has $g_Z = g/\cos\theta_W$, while $g_{Z'}$ is a phenomenologically free parameter. However, in more complete theories involving Z' (*i.e.* GUT or LR models), the value of $g_{Z'}$ is tightly connected to g_Z [2, 7]:

$$g_{Z'} = \sqrt{\frac{5}{3}} \sin\theta_W \sqrt{\lambda} g_Z, \quad (2.2)$$

where λ is usually in the range $2/3$ to 1 [2]. This means that the maximum value is

$$g_{Z'}/g_Z \approx 0.62. \quad (2.3)$$

We shall use this constraint in most of the numerical work that is presented.

Let us write down the Lagrangian for interactions of the Z and Z' with the fermions of the third family:

$$-\mathcal{L}_{ZZ'} = g_Z Z_\mu \sum_{f=tb\tau\nu_\tau} \bar{\psi}_f \gamma^\mu (v_f - a_f \gamma_5) \psi_f + g_{Z'} Z'_\mu \sum_{f=tb\tau\nu_\tau} \bar{\psi}_f \gamma^\mu (v'_f - a'_f \gamma_5) \psi_f. \quad (2.4)$$

The parameters v_f and a_f are defined in the SM as follows:

$$v_f = \frac{1}{2} T_{3L} - \sin^2\theta_W Q, \quad a_f = \frac{1}{2} T_{3L}, \quad (2.5)$$

where T_3 and Q are the third component of weak isospin and of electric charge, respectively (we suppress their flavour indices). The parameters v'_f and a'_f represent the chiral properties of the Z' interactions with fermions and the relative strengths of these interactions. One of all these parameters for all fermions can be absorbed into $g_{Z'}$, and in order to avoid this we normalise $v'^2_\tau + a'^2_\tau = \frac{1}{2}$; this normalization was used in [7] when obtaining Eq. (2.2). However, in our model the quantity $v'^2_f + a'^2_f$ may vary from fermion to fermion. The cancellation of ABJ anomalies restricts the possible choice of v'_f and a'_f and will be discussed in Appendix A.

The weak eigenstates Z_μ and Z'_μ may be mixed so that the mass eigenstates are:

$$\begin{pmatrix} Z_1 \\ Z_2 \end{pmatrix} = \begin{pmatrix} \cos\xi & \sin\xi \\ -\sin\xi & \cos\xi \end{pmatrix} \begin{pmatrix} Z \\ Z' \end{pmatrix}. \quad (2.6)$$

Then the well-known value of the SM Z -boson mass corresponds in this model to the Z_1 mass (M_1), while the mass of the Z_2 boson (M_2) is, of course, unknown.

It is possible to rewrite Eq. (2.4) in terms of the mass eigenstates:

$$\begin{aligned}
-\mathcal{L}_{Z_1 Z_2} = & g_Z \left[Z_{1\mu} \sum_{f=tb\tau\nu_\tau} \bar{\psi}_f \gamma^\mu (v_{f1} - a_{f1} \gamma_5) \psi_f \right. \\
& \left. + Z_{2\mu} \sum_{f=tb\tau\nu_\tau} \bar{\psi}_f \gamma^\mu (v_{f2} - a_{f2} \gamma_5) \psi_f \right], \quad (2.7)
\end{aligned}$$

where

$$\begin{aligned}
v_{f1} &= \cos \xi v_f + \frac{g_{Z'}}{g_Z} \sin \xi v'_f, & a_{f1} &= \cos \xi a_f + \frac{g_{Z'}}{g_Z} \sin \xi a'_f, \\
v_{f2} &= \frac{g_{Z'}}{g_Z} \cos \xi v'_f - \sin \xi v_f, & a_{f2} &= \frac{g_{Z'}}{g_Z} \cos \xi a'_f - \sin \xi a_f. \quad (2.8)
\end{aligned}$$

The introduction of mixing between the Z and Z' changes the couplings of the SM, which are extracted from the conventional experimental input. In fact, in the SM one has the standard electroweak input [16] of $\alpha(0)$, G_F [17] together with $M_Z = (91.1863 \pm 0.002) \text{ GeV}$ [18]. This input contains enough parameters for the determination of the SM electroweak coupling constants g and g' of $SU(2)_L$ and $U(1)_Y$, respectively, and the Higgs vacuum expectation value v . In order to do this let us introduce the following quantities:

$$\mu^2 \equiv \frac{\pi \alpha(0)}{\sqrt{2} G_F} \approx (37.280 \text{ GeV})^2 \quad (2.9)$$

and [19, 20]

$$\rho \equiv \frac{G_F^{\text{NC}}}{G_F^{\text{CC}}} \quad (2.10)$$

where G_F^{NC} is the four-fermion NC Fermi coupling constant in the limit of zero momentum transfer. At the tree level the ρ parameter can be defined as $\rho_0 = M_W^2 / (M_Z^2 \cos^2 \theta_W)$ and in the SM $\rho_0 = 1$ due to the doublet Higgs structure, while at the one-loop level it acquires radiative corrections [19]¹

$$\rho \equiv \frac{1}{1 - \Delta \rho_T}, \quad \Delta \rho_T \approx \frac{3 G_F}{8 \pi^2 \sqrt{2}} m_t^2 \approx 0.01. \quad (2.11)$$

Then it is possible to express the couplings of Eq. (2.4) in terms of the above-mentioned input [15]:

$$g_Z = (4 \sqrt{2} G_F M_Z^2 \rho)^{1/2}, \quad (2.12)$$

¹For $b\bar{b}$ final states there are extra vertex corrections [15].

$$\sin^2 \theta_W = \frac{1}{2} - \sqrt{\frac{1}{4} - \frac{\mu^2}{\rho M_Z^2} \frac{\alpha(M_Z)}{\alpha(0)}}. \quad (2.13)$$

It should be stressed that the angle introduced above differs from the conventionally defined Weinberg angle:

$$\sin^2 \theta_0 \cos^2 \theta_0 = \frac{\mu^2}{M_Z^2} \frac{\alpha(M_Z)}{\alpha(0)}. \quad (2.14)$$

The one-loop expression for this difference can be found in [21].

In the extended model the mass of the weak eigenstate M_Z (*i.e.* the matrix element of the mass operator) is unknown: it is related to the mass values M_1 and M_2 , and to the mixing ξ , as

$$\tan^2 \xi = \frac{M_Z^2 - M_1^2}{M_2^2 - M_Z^2}. \quad (2.15)$$

As a result, *for non-zero mixing angles there are corrections to the Weinberg angle θ_W and gauge couplings g and g' .* They acquire dependence, now not only from the standard electroweak input, but *from the parameters of the extended model (ξ , M_2) as well.* This means that the results of a measurement of other electroweak quantities may be used to restrict these parameters.

Following [15] one finds that in the extended model Eq. (2.13) should be modified by $M_Z \rightarrow M_1$, while the ρ parameter acquires additional contributions at the tree level:

- from the ZZ' mixing ($\Delta\rho_M$):

$$\rho_M = 1 + \sin^2 \xi \left(\frac{M_2^2}{M_1^2} - 1 \right) = \frac{1 + (M_2^2/M_1^2) \tan^2 \xi}{1 + \tan^2 \xi}; \quad (2.16)$$

- from the additional Higgs sector—related to the pattern of symmetry breaking ($\Delta\rho_{SB}$) (the scalar sector of this theory necessarily contains additional Higgs fields),

so that:

$$\begin{aligned} \rho &= \rho_{SB} \cdot \rho_M \cdot \rho_T = \frac{1}{1 - \Delta\rho}, \\ \Delta\rho &= \Delta\rho_{SB} + \Delta\rho_M + \Delta\rho_T, \end{aligned} \quad (2.17)$$

where ρ_{SB} and ρ_M contain tree-level corrections due to the extension of the model, whereas ρ_T contains the SM radiative corrections (dominated by the top quark). Of course, in the extended Z' model there exist additional radiative corrections to the ρ parameter, which can even be rather large since there is no decoupling of the heavy particles for these corrections, but we restrict ourselves by considering only the tree-level effects of the non-standard particles.

If the scalar sector of the theory contains only doublets and singlets of the $SU(2)_L$ group one has $\Delta\rho_{SB} = 0$. In further considerations we shall use this assumption by default.

2.2 Existing bounds on the Z' mass

A Z' would contribute with full strength to the decay of Υ states to $\tau^+\tau^-$, suppressed only by the Z' propagator. The moderate agreement of the branching ratio [17]

$$\text{BR}(\tau) \equiv \frac{\Gamma(\Upsilon(1S) \rightarrow \tau^+\tau^-)}{\Gamma(\Upsilon(1S) \rightarrow \text{all})} = 0.0297 \pm 0.0035, \quad (2.18)$$

with

$$\text{BR}(e) = 0.0252 \pm 0.0017, \quad \text{BR}(\mu) = 0.0248 \pm 0.0007, \quad (2.19)$$

implies that the Z' mass cannot be too low.

Let us estimate this lower bound. Since the $\Upsilon(1S)$ is a natural-parity state, only the vector part of the hadronic current contributes to its decay. Hence, no restriction can be obtained for the pure axial $Z'b\bar{b}$ vertex without ZZ' mixing (such mixing effects are small, and will be omitted from the discussion of $\Upsilon(1S)$ decay). For couplings involving the vector current, one may obtain a lower bound on the Z' mass: $M_{Z'} > 50$ GeV for vector–vector chiralities (in the $Z'b\bar{b}$ and $Z'\tau^+\tau^-$ vertices), $M_{Z'} > 22$ GeV for the vector–axial–vector case, and $M_{Z'} > 35$ GeV for the LL, RR, LR and RL cases.

Another kind of restriction can be obtained from the ρ parameter, as discussed above. If one combines the LEP results with the M_W/M_Z value, it is possible to conclude that [22]

$$2 \cdot 10^{-3} < \Delta\rho < 8 \cdot 10^{-3} \quad \text{for} \quad 150 \text{ GeV} < m_t < 200 \text{ GeV} \quad (2.20)$$

and $70 \text{ GeV} < m_H < 1000 \text{ GeV}$. Under the assumption that $\Delta\rho_{\text{SB}} = 0$, this leads to

$$1 \lesssim \rho_{\text{M}} \lesssim 1.005. \quad (2.21)$$

The lower bound on ρ_{M} implies that $M_2 > M_1$.

However, one should keep in mind that these constraints are valid only under the assumption that $\rho_{\text{SB}} = 1$, which requires a certain simple structure of the Higgs sector. For a more general scalar sector one has [23]

$$\rho_{\text{SB}} = 1 + \frac{\sum_{\text{all } H} \langle H_0^\dagger | (\vec{T}^2 - 3T_3^2) | H_0 \rangle_{\text{vac}}}{2 \sum_{\text{all } H} \langle H_0^\dagger | T_3^2 | H_0 \rangle_{\text{vac}}}. \quad (2.22)$$

For Higgs fields with isospin higher than $1/2$, ρ_{SB} may be less than unity and the above-mentioned constraints are removed.

3 Hadronic production

The hypothetical Z' boson could be produced in proton–proton (antiproton) collisions through direct Drell–Yan-like coupling of b and \bar{b} sea quarks, through gluon–gluon fusion, with the gluons coupled to b or t quark loops, as well as through ZZ fusion and WW fusion. We shall consider these mechanisms in turn in the following, focusing first on the prospects for producing such vector bosons at the Fermilab Tevatron, and then turn to the LHC in Sect. 3.4. In this section we consider the limit of no ZZ' mixing, which implies $M_{Z'} = M_2$. Also, we shall here disregard the constraint (2.3), letting Z' couplings be of $\mathcal{O}(1)$.

3.1 Direct production by $b\bar{b}$ annihilation

The vector boson Z' may be produced by the direct Drell–Yan mechanism, *i.e.* annihilation of a b quark from one proton (or antiproton) and a \bar{b} from the other. The matrix element is proportional to

$$M = g_{Z'}^2 [\bar{v}(p_2)\gamma^\mu(v'_b - a'_b\gamma_5)u(p_1)] \frac{-g_{\mu\nu} + k_\mu k_\nu/M_{Z'}^2}{k^2 - M_{Z'}^2 + iM_{Z'}\Gamma_{Z'}} [\bar{u}(q)\gamma^\nu(v'_q - a'_q\gamma_5)v(\bar{q})], \quad (3.1)$$

where p_1 and p_2 are the relevant parton momenta of the incident proton and antiproton, with $k = p_1 + p_2$, and q and \bar{q} the final-state quark and antiquark momenta. The corresponding polarisation-averaged square becomes

$$\begin{aligned} \overline{|M|^2} &= \frac{4g_{Z'}^4}{(k^2 - M_{Z'}^2)^2 + (M_{Z'}\Gamma_{Z'})^2} \{X_0 + m_b^2 X_b + m_q^2 X_q + m_b^2 m_q^2 X_{bq} \\ &\quad + m_b^4 X_{bb} + m_q^4 X_{qq}\}, \end{aligned} \quad (3.2)$$

where m_q ($= m_b$ or m_t) denotes the mass of the final-state quarks and

$$\begin{aligned} X_0 &= \frac{1}{2}(v_b'^2 + a_b'^2)(v_q'^2 + a_q'^2)(\hat{t}^2 + \hat{u}^2) + 2v_b'a_b'v_q'a_q'\hat{s}(\hat{t} - \hat{u}), \\ X_b &= (v_q'^2 + a_q'^2)[3(v_b'^2 + a_b'^2)(\hat{s} + 2\hat{t}) + 2v_b'^2\hat{s}] + 12v_b'a_b'v_q'a_q'\hat{s}, \\ X_q &= (v_b'^2 + a_b'^2)[3(v_q'^2 + a_q'^2)(\hat{s} + 2\hat{t}) + 2v_q'^2\hat{s}] + 12v_b'a_b'v_q'a_q'\hat{s}, \\ X_{bq} &= 4\{v_b'^2 v_q'^2 + a_b'^2 a_q'^2[3 - 2(\hat{s}/M_{Z'}^2) + (\hat{s}/M_{Z'}^2)^2]\}, \\ X_{bb} &= X_{qq} = 2(v_b'^2 + a_b'^2)(v_q'^2 + a_q'^2), \end{aligned} \quad (3.3)$$

with $\hat{s} = k^2$, $\hat{t} = (p_1 - q)^2$, and $\hat{u} = (p_1 - \bar{q})^2$.

For the decay of the Z' (of mass $M_{Z'}$) to a fermion–antifermion pair (of mass m_f), we find the partial decay width at the tree level

$$\Gamma_f = \frac{g_{Z'}^2 M_{Z'}}{12\pi} \sqrt{1 - (2m_f/M_{Z'})^2} \left[v_f'^2 \left(1 + \frac{2m_f^2}{M_{Z'}^2}\right) + a_f'^2 \left(1 - \frac{4m_f^2}{M_{Z'}^2}\right) \right], \quad (3.4)$$

where v'_f and a'_f denote the vector and axial couplings, respectively. Thus, the total fermionic width would be given by

$$\Gamma_{Z'} = \Gamma_b + \Gamma_t + \Gamma_\tau + \Gamma_{\nu_\tau}. \quad (3.5)$$

The inclusive cross section may be expressed in terms of a convolution integral over b -quark distribution functions:

$$\frac{d\sigma}{dE_\perp} = \int dx_1 \int dx_2 \frac{d^3\hat{\sigma}}{dE_\perp dx_1 dx_2} f_1^b(x_1) f_2^{\bar{b}}(x_2), \quad (3.6)$$

with E_\perp the transverse energy of the jets, and $f_i^q(x)$ the b (\bar{b})-quark distribution functions. The elementary cross section is given by

$$\frac{d^8\hat{\sigma}}{dx_1 dx_2} = (2\pi)^4 \delta^{(4)}(p_1 + p_2 - q - \bar{q}) \frac{1}{4E_1 E_2 v_{\text{rel}}} \overline{|M|^2} \frac{d^3 q}{(2\pi)^3 2E_q} \frac{d^3 \bar{q}}{(2\pi)^3 2E_{\bar{q}}}, \quad (3.7)$$

with $\overline{|M|^2}$ the square of the matrix element in Eq. (3.2), properly averaged and summed over polarisations, and $4E_1 E_2 v_{\text{rel}} = 2(p_1 + p_2)^2 \equiv 2\hat{s}$. Straightforward kinematical considerations lead to:

$$\frac{d^3\hat{\sigma}}{dE_\perp dx_1 dx_2} = \frac{1}{2\pi} \frac{1}{8\hat{s}^{3/2}} \overline{|M|^2} \frac{E_\perp}{\sqrt{E_q^2 - E_\perp^2} \cosh y - E_q \sinh y}, \quad (3.8)$$

where y is the rapidity and

$$\left. \begin{matrix} E_q \\ E_{\bar{q}} \end{matrix} \right\} = \frac{1}{2} \sqrt{\hat{s}} \left[\cosh y \pm \sinh y \sqrt{1 - 4E_\perp^2/\hat{s}} \right]. \quad (3.9)$$

It is convenient to replace the integration over x_1 and x_2 by one over rapidity and \hat{s} , the invariant mass squared of the Z' . With $\tau \equiv \hat{s}/s$, where s is the squared c.m. energy of the proton-antiproton system, we have $x_1 = \sqrt{\tau} e^y$ and $x_2 = \sqrt{\tau} e^{-y}$, and obtain

$$\frac{d\sigma}{dE_\perp} = \frac{1}{2\pi} \frac{1}{8s} \int \frac{d\hat{s}}{\hat{s}\sqrt{\hat{s}}} \int dy \overline{|M|^2} f_1^b(x_1) f_2^{\bar{b}}(x_2) \frac{E_\perp}{\sqrt{E_q^2 - E_\perp^2} \cosh y - E_q \sinh y}, \quad (3.10)$$

where $\overline{|M|^2}$ is obtained from Eq. (3.2).

Resulting cross sections are given in Fig. 1 for the Fermilab energy, $\sqrt{s} = 1.8$ TeV, for three values of the mass, $M_{Z'} = 100, 200$ and 400 GeV. We here disregard the constraint (2.3), taking the more ‘unbiased’ view that $g_{Z'} a'$ and $g_{Z'} v'$ are of $\mathcal{O}(1)$. (If we adopt Eq. (2.3), the cross section would drop by about two orders of magnitude.) For the distribution of b (\bar{b}) quarks in the incident protons and antiprotons, we use standard values [24, 25]. For comparison, we also show the dominant QCD contributions [cf. Appendix B] and data (summed over all flavours) [26]. The direct $b\bar{b}$ production through a Z' is seen to be below the QCD rate by 3–4 orders of magnitude, even for a ‘light’ Z' .

3.2 Gluon fusion

In the collisions of protons and antiprotons at Fermilab (or protons at LHC), gluon fusion may, via a suitable quark triangle diagram, lead to production of such Z' bosons. The inclusive cross section may be expressed in terms of a convolution integral over gluon distribution functions, similar to Eq. (3.6):

$$\frac{d\sigma}{dE_\perp} = \int dx_1 \int dx_2 \frac{d^3\hat{\sigma}}{dE_\perp dx_1 dx_2} f_1^g(x_1) f_2^g(x_2) \quad (3.11)$$

with $f_i^g(x)$ gluon distribution functions. The elementary cross section is given by an expression similar to Eq. (3.7), where the amplitude for the production of $q\bar{q}$ ($b\bar{b}$ or $t\bar{t}$) final states may be expressed as

$$M = V_{\mu\alpha\beta}^{ab} \epsilon^\alpha(1) \epsilon^\beta(2) g_{Z'} \frac{-g^{\mu\nu} + k^\mu k^\nu / M_{Z'}^2}{k^2 - M_{Z'}^2 + iM_{Z'} \Gamma_{Z'}} [\bar{u}(q) \gamma_\nu (v'_q - a'_q \gamma_5) v(\bar{q})]. \quad (3.12)$$

The factor $V_{\mu\alpha\beta}^{ab}$ describes the $Z'gg$ vertex (a and b are colour indices), which we take from the corresponding expression for the Zgg vertex, given by Kniehl and Kühn [27].

By current conservation, $k^\nu [\bar{u}(q) \gamma_\nu v(\bar{q})] = 0$. Furthermore, for on-shell gluons, the vertex function simplifies considerably. Averaging over gluon polarisations, and summing over q and \bar{q} polarisations, we obtain

$$\overline{|M|^2} = 4a_Q'^2 g_{Z'}^4 \left(\frac{\alpha_s}{\pi}\right)^2 \delta^{ab} |B_Q|^2 \left(\frac{\hat{s}}{M_{Z'}^2}\right)^2 a_q'^2 m_q^2 \hat{s}. \quad (3.13)$$

Here, a_Q' describes the axial coupling of Z' to the quark field of the triangle diagram, normalised as in Sect. 2. (If we were to replace the Z' by the ordinary Z , we would get $a_Q' g_{Z'} \rightarrow eT_3/(2\sin\theta_W \cos\theta_W)$, with $T_3 = \pm\frac{1}{2}$ the quark isospin.) The coefficient B_Q is given in Ref. [27]. For a triangle diagram of quark flavour Q , it is

$$B_Q = \frac{\hat{s}}{2\lambda} (1 - 2m_Q^2 C_0), \quad (3.14)$$

with $\lambda = \lambda(s_1, s_2, \hat{s}) = \hat{s}^2$ the Källén function (for on-shell gluons, $s_1 = s_2 = 0$), m_Q the mass of the loop quark, and C_0 given as

$$\begin{aligned} C_0 &= \frac{1}{2\hat{s}} (2\phi - \pi)^2, & \sin\phi &= \sqrt{4m_Q^2/\hat{s} - 1}, & \hat{s} &< 4m_Q^2, \\ C_0 &= -\frac{1}{2\hat{s}} \left(\log \frac{1+\hat{a}}{1-\hat{a}} - i\pi \right)^2, & \hat{a} &= \sqrt{1 - 4m_Q^2/\hat{s}} < 1, & 4m_Q^2 &< \hat{s}, \end{aligned} \quad (3.15)$$

depending on whether \hat{s} is below or above the threshold associated with the loop quark. We consider the contributions from both b and t quarks to this loop:

$$a_Q'^2 |B_Q|^2 \rightarrow |a_b' B_b + a_t' B_t|^2. \quad (3.16)$$

The result (3.13) is proportional to $a_q'^2 m_q^2$. According to Furry's theorem, the vector part of the triangle diagram cancels, and the remaining axial anomaly is proportional to the final-state quark mass, here denoted by m_q . At moderate energies, the relevant final states are $b\bar{b}$, thus $m_q = m_b$. If the energy is high enough, there is a similar contribution for $t\bar{t}$ final states.

Replacing the integrations over x_1 and x_2 by integrations over rapidity and \hat{s} , the invariant mass squared of the Z' , one obtains an expression similar to Eq. (3.10), where the b and \bar{b} distribution functions should be replaced by gluon distribution functions, and where $|\overline{M}|^2$ also should contain a factor $1/8$ from colour matching of the two gluons.

Numerical values are obtained for these cross sections, using standard gluon distribution functions [24, 25]. The resulting cross sections are for the Tevatron energy shown in Fig. 2. We have arbitrarily taken the axial couplings to b and t quarks to be the same. The cross section is remarkably small, even for moderately low masses, $M_{Z'} \simeq \mathcal{O}(M_Z)$. The resonant structure is due to interference between the contributions of b - and t -quark triangle diagrams, cf. Eq. (3.16). This interference is illustrated in Fig. 3, where for $M_{Z'} = 200$ GeV we compare three cases: (1) the $b\bar{b}Z'$ and $t\bar{t}Z'$ axial couplings being the same (solid), (2) opposite (dashed), and (3) the $t\bar{t}Z'$ axial coupling being zero. It appears that no variation of the chirality of these couplings can make the cross section comparable with the QCD background.

3.3 Fusion of ZZ or WW bosons

The fusion of two weak gauge bosons, like that of two gluons, can also lead to Z' production. This could proceed through mixing, or via a triangle loop. A crude estimate for the magnitude of this rate may be obtained in the Weizsäcker–Williams approximation. The resulting cross section is found to be several orders of magnitude below the Drell–Yan rate.

3.4 Production at the LHC

At the LHC the sea-quark and gluon distributions are much less suppressed than at the ‘lower’ energy of the Tevatron, so it is of considerable interest to see if the Z' production can compete with the QCD background. We show in Figs. 4 and 5 the cross sections for $b\bar{b}$ Drell–Yan-type production and gluon fusion, respectively. As at lower energies, it is the Drell–Yan-type production that dominates the gluon-fusion mechanism and, relative to the QCD rate, the Z' production is now ‘only’ suppressed by about two orders of magnitude. One must conclude that it would be extremely hard to discover such vector bosons in hadronic collisions.

4 Electron–positron annihilation

In e^+e^- collisions the Z' boson could be produced directly via mixing with the Z boson; the following channels with two-particle final states are sensitive to this mixing:

$$e^+e^- \rightarrow b\bar{b}; \quad e^+e^- \rightarrow t\bar{t}; \quad e^+e^- \rightarrow \tau\bar{\tau}. \quad (4.1)$$

The first of these was discussed in [7, 11]. In the following subsection we are going to discuss all these processes and calculate the relative deviation of the cross sections from their values in the SM for different values of the mixing angle ξ and the Z_2 mass M_2 .

For the processes with more than two particles in the final state we will consider the process $e^+e^- \rightarrow b\bar{b}\nu_e\bar{\nu}_e$ as one of the most important for LEP2 and future colliders.

4.1 Two-fermion final states

We first consider the processes $e^+e^- \rightarrow b\bar{b}$, $t\bar{t}$, $\tau^+\tau^-$ as the simplest processes at electron–positron colliders involving fermions of the third family, where the effect of Z' exchange could be observable. Three Feynman diagrams describe this process, with the exchange of photons, Z_1 and Z_2 . Deviations from the SM will occur only in the case where the mixing angle is non-zero. (Without tree-level mixing, it will arise only through loop effects.) The effect of ZZ' mixing changes the couplings of the Z boson and gives rise to Z_2 exchange. The coupling between the electron and the Z' is proportional to $\sin\xi$, which by assumption is small. On the other hand, this mechanism has the advantage that there is no suppression by the Z' propagator and the effect might thus be observable.

The cross section is given by the expression (for $m_f \ll \sqrt{s}$):

$$\sigma_{f\bar{f}} = \frac{4\pi\alpha^2}{3s} F_1, \quad (4.2)$$

where

$$\begin{aligned} F_1 = & Q_e^2 Q_f^2 + 2Q_e \bar{\nu}_{e1} Q_f \bar{\nu}_{f1} \text{Re}\chi_1 + (\bar{\nu}_{e1}^2 + \bar{a}_{e1}^2)(\bar{\nu}_{f1}^2 + \bar{a}_{f1}^2)|\chi_1|^2 \\ & + 2Q_e \bar{\nu}_{e2} Q_f \bar{\nu}_{f2} \text{Re}\chi_2 + (\bar{\nu}_{e2}^2 + \bar{a}_{e2}^2)(\bar{\nu}_{f2}^2 + \bar{a}_{f2}^2)|\chi_2|^2 \\ & + 2(\bar{\nu}_{e1}\bar{\nu}_{e2} + \bar{a}_{e1}\bar{a}_{e2})(\bar{\nu}_{f1}\bar{\nu}_{f2} + \bar{a}_{f1}\bar{a}_{f2})\text{Re}\chi_1\chi_2^*, \end{aligned} \quad (4.3)$$

with

$$\chi_i = \frac{s}{s - M_i^2 + iM_i\Gamma_i}, \quad (4.4)$$

and [cf. Eq. (2.8)]

$$\bar{v}_i = \frac{g_Z}{e} v_i, \quad \bar{a}_i = \frac{g_Z}{e} a_i. \quad (4.5)$$

The ratio g_Z/e should be extracted from the standard electroweak input discussed in Sect. 2, and include the ‘running’ dependence from the e^+e^- energy \sqrt{s} .

For $\sqrt{s} = M_1$ one can use the following [15, 16]

$$\frac{g_Z}{e}(M_1^2) = \frac{1}{\sin \theta_W \cos \theta_W} \Big|_{\sqrt{s}=M_Z} = \left[\frac{M_1^2 \rho \alpha(0)}{\mu^2 \alpha(M_1)} \right]^{1/2}. \quad (4.6)$$

For $\sqrt{s} > M_1$ we will start with (4.6) and then use the solutions of the one-loop massless renormalization-group equations for the $SU(2)$ and $U(1)$ running couplings, g and g' :

$$\begin{aligned} g^2(s) &= g^2(M_1^2) \left(1 + \frac{g^2(M_1^2)}{16\pi^2} \frac{10}{3} \log \frac{s}{M_1^2} \right)^{-1}, \\ g'^2(s) &= g'^2(M_1^2) \left(1 - \frac{g'^2(M_1^2)}{16\pi^2} \frac{20}{3} \log \frac{s}{M_1^2} \right)^{-1}, \end{aligned} \quad (4.7)$$

which are related to e and $\sin \theta_W$ as

$$e^2 = \frac{g^2 g'^2}{g^2 + g'^2}, \quad \sin^2 \theta_W = \frac{g'^2}{g^2 + g'^2}. \quad (4.8)$$

It should be emphasised that all the above-mentioned couplings depend, for the model under consideration, on the mixing angle ξ and the mass M_2 through the ρ parameter, cf. Eqs. (4.6) and (4.7).

No deviation from the SM has been observed at LEP. One may thus obtain bounds on the model parameters ξ and M_2 , taking into account available data on the Z^0 peak. For LEP2 and the NLC we take a rather conservatively anticipated precision. The sensitivity of observables, e.g. of the total cross section $\sigma_{f\bar{f}}$, has been assessed numerically by defining a χ^2 function as follows:

$$\chi^2 = \left(\frac{\Delta \sigma_{f\bar{f}}}{\delta \sigma_{f\bar{f}}} \right)^2, \quad (4.9)$$

where $\Delta \sigma_{f\bar{f}} = \sigma_{f\bar{f}} - \sigma_{f\bar{f}}^{\text{SM}}$ and the uncertainty $\delta \sigma_{f\bar{f}}$ is the statistical one. As a criterion to derive allowed regions for the coupling constants if no deviations from the SM were observed, and in this way to assess the sensitivity to the parameters ξ and M_2 , we impose that $\chi^2 < \chi_{\text{crit}}^2$, where χ_{crit}^2 is a number that specifies the desired level of significance.

At the Z^0 peak, the most sensitive quantity is the forward–backward asymmetry. The resulting allowed bounds on ξ and M_2 , at the 95% C.L., are given

for $b\bar{b}$ and $\tau^+\tau^-$ production in Figs. 6–8, for different assumed chiralities of the coupling to the Z' (vector, axial, left, right). The relative gauge coupling is chosen according to [2] as $g_{Z'}/g_Z \simeq 0.62$. These bounds were obtained from the data reported in [30], by means of the program ZEFIT, which has to be used along with ZFITTER [31].

In these same figures, we also present bounds corresponding to conservatively assumed cross-section precisions of 5% and 10% at LEP2 and a linear collider operating at 500 GeV (labelled NLC). These cross sections were calculated by means of the CompHEP [32] program. The qualitative difference between the LEP1 and the LEP2 (or NLC) contours is due to the following. At LEP1 (on resonance) there are three effects: modification of the couplings due to mixing, modification of $\sin^2\theta_W$, and a shift of ρ from the SM value. The corresponding bounds are smooth curves. At higher energies (LEP2 and NLC) there is an additional contribution mediated by Z_2 exchange. At relatively low M_2 values, the Z_2 -exchange contribution dominates the deviation from the SM, whereas at higher M_2 this contribution becomes less important. The complicated shape of the contours is due to interference between direct (Z_2 exchange) and indirect effects. These effects interfere constructively at some values of $\sin\xi$, and destructively at others.

In our input scheme, for a fixed non-zero value of ξ , the gauge coupling g_Z increases with M_2 . This is due to the increase of ρ_M , and hence of ρ [cf. Eqs. (2.12), (2.16) and (2.17)] with M_2 . This leads to a deviation of the cross section away from the SM value. Thus, at large values of M_2 , the $e^+e^- \rightarrow f\bar{f}$ cross section is seen to impose strong constraints on the allowed mixing angle; there is a narrowing, at large M_2 , of the allowed region in $\sin\xi$. (If we had frozen ρ and g_Z in our calculations, then the different points in these figures would correspond to different choices of Higgs sector—which would be rather unnatural.)

For the case of $b\bar{b}$ final states, we consider two different centre-of-mass energies, $\sqrt{s} = 190$ and 500 GeV, in Figs. 6 and 7, respectively. The sensitivity of LEP2 and the NLC to ξ and M_2 depends on the chiral property of the Z' coupling. For vector-, axial vector- and left-handed couplings, LEP2 (and the NLC) will have more sensitivity than LEP1 at negative values of ξ . For right-handed couplings, the situation is reversed. Thus, LEP2 and the NLC have the potential to observe effects of such a Z' in this channel with masses up to the order of 1 TeV. Concerning $\tau^+\tau^-$ final states, it appears that studies at higher energies cannot improve on the results obtained at LEP1, see Fig. 8.

In Fig. 9 we consider $t\bar{t}$ final states at $\sqrt{s} = 500$ GeV. As compared with $b\bar{b}$ final states, the sensitivity is lower. However, the interference effects are different, and it is therefore complementary to the $b\bar{b}$ channel.

Comparing the contour levels for the different final states, one can see that the tightest restrictions are obtained from the $b\bar{b}$ final state, while the $\tau^+\tau^-$ case is the least restrictive. This difference can be understood from an analysis of the expression (4.3). In comparing with the SM cross section, the important

difference between the final-state fermions is the electric charge, which dominates the main SM contribution. Thus, for a given value of (ξ, M_2) away from the resonance $\sqrt{s} = M_2$, the relative deviation from the SM will be largest for b quarks (because of the small electric charge) and smallest for τ leptons (because of the large electric charge).

4.2 Four-fermion final states

We now turn our attention to the process $e^+e^- \rightarrow b\bar{b}\nu_e\bar{\nu}_e$, which is sensitive to the three-boson couplings. In the SM, there are in the unitary gauge 23 Feynman diagrams that contribute to this process. In the extended model, the number of diagrams is 48 (in the unitary gauge), even if all the scalars are excluded. However, deviations from the standard model occur only for the case of a non-zero ZZ' mixing². As a result of this mixing there appear three-boson couplings involving the Z_2 .

Experimentally this process can be investigated by the detection of the $b\bar{b}$ pair with missing energy. In this case one measures the cross section of the processes $e^+e^- \rightarrow b\bar{b}\nu_i\bar{\nu}_i$, integrated over a suitable kinematical region (with the neutrinos of all three families in the final state). However, following the work of Ref. [33], we believe that the main contribution comes from the process with the $\nu_e\bar{\nu}_e$ pair in the final state.

The process has been studied using CompHEP, which generates the Feynman diagrams (we omit virtual Higgs particles) and evaluates the cross section. This has been integrated over phase space according to the cuts of Ref. [33]. For the b jets to be detectable, we require them to have sufficient energy, to be away from the beam pipe, not too close to each other, and not have an invariant mass close to the Z_1 . Furthermore, the missing momentum should have a large transverse component and a low rapidity, and the undetected neutrinos should not originate from a Z_1 :

$$\begin{aligned} E_b &> 20 \text{ GeV}, & 20^\circ < \theta_b < 160^\circ, \\ \theta_{b\bar{b}} &> 20^\circ, & |m_{b\bar{b}} - m_{Z_1}| < 3\Gamma_Z \\ p_T &> 40 \text{ GeV}, & \eta(p) < 1, \\ |\not{p} - m_{Z_1}| &> 5\Gamma_Z. \end{aligned} \tag{4.10}$$

At a given energy, the cross section increases significantly with increasing values of M_2 , and also with $|\sin \xi|$, as is shown in Fig. 10. The increase in the cross section seen at increasing values of M_2 is basically due to the fact that the coupling g_Z increases through the increase of the ρ_M parameter, as was discussed in Sect. 4.1.

²There is no tree-level WWZ' coupling since we assume the Z' is an $SU(2)$ singlet. One should keep in mind that the one-loop Feynman diagrams give rise to a WWZ' vertex even if at the tree level the mixing angle vanishes.

For the cases of $\sqrt{s} = 190$ and 500 GeV, and for vector couplings, the modifications of the cross sections, with respect to the Standard Model, are given in Figs. 11 and 12, respectively. The gross features of these figures are rather similar to those for the $b\bar{b}$ final states, and the sensitivity is quite comparable.

5 Concluding remarks

We have shown that a Z' boson coupled only to the third-family fermions is rather difficult to discover, even at high-energy colliders, thus confirming the more exploratory analysis of Ref. [11].

For hadronic colliders, such as the Tevatron or the LHC, this Z' is invisible because of the QCD background, which is many orders of magnitude greater than the cross sections involving the Z' . The data available from LEP1 already exclude significant regions of the parameter space (ξ, M_2) . LEP2 and future e^+e^- linear colliders can improve on these bounds, in particular from studies of final states involving $b\bar{b}$.

It seems that some additional progress may be achieved in the study of processes with four fermions in the final state, if one investigates not only the full cross sections, but also their dependence from the $b\bar{b}$ ($t\bar{t}$, $\tau\bar{\tau}$) invariant mass. We hope to return to this question in future work.

Acknowledgements

It is a pleasure to thank Alexander Pukhov for instructing us on how to use CompHEP, and Wolfgang Hollik for valuable discussions. This research has been supported by the Research Council of Norway, and by the Nordic project (NORDITA) ‘Fundamental constituents of matter’. Also, A.A. and N.R. are partially supported by grant RFFI 98-02-18137.

Appendix A: Higgs sector and anomalies

Since we consider our model as an extension of the Standard Model, it should contain the standard Higgs doublet:

$$H = \frac{1}{\sqrt{2}} \begin{pmatrix} h^+ \\ v + h^0 \end{pmatrix} \quad (\text{A.1})$$

where v is the vacuum expectation value. This field realizes the representation $(1/2, 1, 0)$ of the gauge group $SU(2)_L \times U(1)_Y \times U(1)_{Y'}$ and hence has the following covariant derivative:

$$D_\mu H = \left(\partial_\mu + igT^a W_\mu^a + i\frac{g'}{2} B_\mu \right) H. \quad (\text{A.2})$$

The kinetic term for this field contributes to the mass terms of the W^\pm and Z bosons:

$$\begin{aligned} |D_\mu H|^2 &\implies \frac{v^2}{8} (gW_\mu^3 - g'B_\mu)^2 + \frac{v^2}{2} g^2 W_\mu^+ W^{\mu-} \\ &= \frac{v^2}{8} \frac{g^2}{\cos^2 \theta_W} Z_\mu Z^\mu + \frac{v^2}{2} g^2 W_\mu^+ W^{\mu-}. \end{aligned} \quad (\text{A.3})$$

This field does not supply the additional gauge boson Z' with a mass. It is impossible to assign to the field H a non-zero Y' hypercharge: in this case the mass terms for the fermions of the first two families will lose the $U(1)_{Y'}$ invariance. Therefore $Y'_H = 0$ and in our model the field H could give rise to the masses of the third-family fermions only in the case when $Y'_{fL} = Y'_{fR}$ (not necessarily zero). In the general case, when $Y'_{fL} \neq Y'_{fR}$, the ordinary Higgs field H does not contribute to the masses of the third-family fermions.

The simplest way to obtain a Z' mass is to introduce a scalar singlet ϕ , which transforms as $(0, 0, Y'_S)$ and has a covariant derivative:

$$D_\mu \phi = \left(\partial_\mu + ig_{Z'} \frac{Y'_S}{2} Z'_\mu \right) \phi. \quad (\text{A.4})$$

With a non-vanishing vacuum expectation value, $\langle \phi \rangle_{\text{vac}} = v_S / \sqrt{2}$, it produces the following mass term for the Z' boson:

$$|D_\mu \phi|^2 \implies \frac{g_{Z'}^2}{8} Y_S'^2 v_S^2 Z_\mu'^2. \quad (\text{A.5})$$

By means of this field ϕ , an arbitrary mass can produced for the Z' boson, but it is not possible to get ZZ' mixing at the tree level. In the case where the Z' boson is not a pure vector particle [$Y'_{fL} \neq Y'_{fR}$], it is also impossible to obtain gauge-invariant mass terms for the fermions of the third family (see above).

In order to solve these two problems, let us introduce an additional Higgs doublet H_1 , which interacts with the Z' and hence has a non-zero Y' hypercharge. This field transforms as $(\frac{1}{2}, 1, Y'_1)$ and has a covariant derivative:

$$D_\mu H_1 = \left(\partial_\mu + igT^a W_\mu^a + i\frac{g'}{2}B_\mu + i\frac{g_{Z'}}{2}Y'_1 Z'_\mu \right) H_1. \quad (\text{A.6})$$

(The value of Y'_1 is not arbitrary when the field H_1 gives rise to fermion masses, this will be discussed at the end of this appendix.) With $\langle H_1 \rangle_{\text{vac}} = v_1/\sqrt{2}$, it produces the following contribution to the mass term of the neutral gauge bosons:

$$|D_\mu H_1|^2 \Rightarrow \frac{g^2}{\cos^2 \theta_W} \frac{v_1^2}{8} \left(Z_\mu^2 + \frac{g_{Z'}^2}{g'^2} \sin^2 \theta_W Y_1'^2 Z_\mu'^2 - 2 \frac{g_{Z'}}{g'} \sin \theta_W Y'_1 Z_\mu Z'^\mu \right). \quad (\text{A.7})$$

So in this case when all three Higgs fields are present, one obtains a mass matrix for the neutral gauge bosons in the general form:

$$(Z, Z') \begin{pmatrix} M_Z^2 & M_{ZZ'}^2 \\ M_{ZZ'}^2 & M_{Z'}^2 \end{pmatrix} \begin{pmatrix} Z \\ Z' \end{pmatrix}, \quad (\text{A.8})$$

where

$$M_Z^2 = \frac{g^2}{4 \cos^2 \theta_W} (v^2 + v_1^2); \quad M_{Z'}^2 = \frac{g_{Z'}^2}{4} (v_S^2 Y_S^2 + v_1^2 Y_1^2), \quad (\text{A.9})$$

$$M_{ZZ'}^2 = -\frac{g^2}{\cos^2 \theta_W} \frac{v^2}{4} \frac{g_{Z'}}{g'} \sin \theta_W Y_1. \quad (\text{A.10})$$

After the diagonalization of this matrix, the mass eigenstates M_1 , M_2 and the mixing angle ξ can be expressed through v.e.v.'s of the introduced scalars. The field H_1 also gives masses to the third-family fermions.

However it should be stressed that the values of the Y' hypercharge are not arbitrary: restrictions come from the triangle anomalies. The well-known condition of ABJ anomalies reads [34, 35]:

$$\text{Tr}(T_i \{T_j, T_k\})_L = \text{Tr}(T_i \{T_j, T_k\})_R \quad (\text{A.11})$$

where T are the matrices of the fermion representations, and i, j, k may refer to different subgroups of the full gauge group.

In the Standard Model with the group $SU(3)_c \times SU(2)_L \times U(1)_Y$, these conditions unambiguously fix ratios of electric charges (or hypercharges) of fermions: four independent conditions of diagrams with LLY , YYY , ccY and ggY external fields (here L denotes the $SU(2)_L$ field, Y the $U(1)_Y$ field, c the $SU(3)$ field, and g the graviton) for four ratios of Y_{L_L} , Y_{e_R} , Y_{q_L} , Y_{u_R} , Y_{d_R} have a single solution. For the extended model, there are additional conditions: LLY' , YYY' ,

$YY'Y'$, $Y'Y'Y'$, ccY' and ggY' , which necessarily lead to $Y' = Y$. All other Y' assignments need an extension of the fermionic sector. In order not to introduce exotic fermions let us consider the simplest extension of the fermionic sector, namely addition of right-handed neutrinos. In this case the anomaly cancellation conditions, involving the Z' boson read:

$$\begin{aligned}
LLY' : \quad & Y'_{\mathcal{L}L} + 3Y'_{\mathcal{Q}L} = 0, \\
ccY' : \quad & 3(2Y'_{\mathcal{Q}L} - Y'_{tR} - Y'_{bR}) = 0, \\
ggY' : \quad & 2Y'_{\mathcal{L}L} - Y'_{\tau R} - Y'_{\nu R} + 3(2Y'_{\mathcal{Q}L} - Y'_{tR} - Y'_{bR}) = 0, \\
Y'Y'Y' : \quad & 2Y'^3_{\mathcal{L}L} - Y'^3_{\tau R} - Y'^3_{\nu R} + 3(2Y'^3_{\mathcal{Q}L} - Y'^3_{tR} - Y'^3_{bR}) = 0, \\
YYY' : \quad & 2Y'_{\mathcal{L}L} - 4Y'_{\tau R} + 3\left(\frac{2}{9}Y'_{\mathcal{Q}L} - \frac{16}{9}Y'_{tR} - \frac{4}{9}Y'_{bR}\right) = 0, \\
YY'Y' : \quad & -2Y'^2_{\mathcal{L}L} + 2Y'^2_{\tau R} + 3\left(\frac{2}{3}Y'^2_{\mathcal{Q}L} - \frac{4}{3}Y'^2_{tR} + \frac{2}{3}Y'^2_{bR}\right) = 0.
\end{aligned} \tag{A.12}$$

Here, \mathcal{L} and \mathcal{Q} denote the third-family lepton and quark doublets. The last two equations are not independent. With $x_i \equiv Y'_i/Y'_{\mathcal{L}L}$, the system has the following solution:

$$\begin{aligned}
x_{\mathcal{L}L} &= 1, & x_{\mathcal{Q}L} &= -\frac{1}{3}, & x_{\tau R} &= 2 - x_{\nu R}, \\
x_{bR} &= \frac{2}{3} - x_{\nu R}, & x_{tR} &= -\frac{4}{3} + x_{\nu R},
\end{aligned} \tag{A.13}$$

where $Y'_{\nu R}$ (or $x_{\nu R}$) remains undetermined. For the case $x_{\nu R} = 0$ one gets $Y = Y'$ (case of the SM), whereas $x_{\nu R} = 1$ corresponds to a purely vector Z' boson; the general case can be treated as a linear combination of these two cases.

These values of fermionic hypercharges Y'_i determine the hypercharge Y'_1 of the H_1 field: the gauge invariance of the fermionic mass term necessarily leads to $Y'_1 = Y'_{\mathcal{L}L} - Y'_{\tau R}$.

A vector-like Z' -fermion coupling is achieved with a universal choice: $x_{\nu R} = 1$. However, as follows from Eqs. (A.13), the assignment for the Z' -fermion vertex to be axial, left- or right-handed cannot be done universally. For instance, the coupling may be purely axial either for b quarks, or for τ leptons, or for t quarks, but not simultaneously.

Let us now comment on the chirality choices considered in Figs. 6–9. For the $Z'b\bar{b}$ coupling (Figs. 6 and 7) to be vector, axial, left- or right-handed, one must choose $x_{\nu R} = 1, 1/3, 2/3$, or $-\infty$, respectively. For the $Z'\tau^+\tau^-$ coupling (Fig. 8) to be vector, axial, left- or right-handed, one must choose $x_{\nu R} = 1, 3, 2$, or $-\infty$, respectively. For the $Z't\bar{t}$ coupling (Fig. 9) to be vector, axial, left- or right-handed, one must choose $x_{\nu R} = 1, 5/3, 4/3$, or ∞ , respectively.

It may be useful to notice that the cancellation of anomalies is necessary only if the additional Z' boson is treated as a fundamental particle. For a composite Z' , arbitrary values of fermionic hypercharge are allowed.

Appendix B: QCD background

We shall assume that light-flavour quark jets can be rejected and do not constitute a background. Thus, the background of interest is the one due to $b\bar{b}$ (and, at sufficiently high energies, $t\bar{t}$) jets.

B.1 Quark–antiquark annihilation

With $p_1 + p_2 = b + \bar{b}$, $\hat{s} = (p_1 + p_2)^2$, the matrix element can be written as

$$M = \bar{v}(p_2)\gamma^\mu g T_a u(p_1) \frac{-g_{\mu\nu}}{\hat{s}} \bar{u}(b)\gamma^\nu g T_b v(\bar{b}) \delta_{ab}, \quad (\text{B.1})$$

with g the QCD coupling. Properly averaged over spin and colour, the squared matrix element takes the form:

$$\overline{|M|^2} = \frac{8}{9} \frac{g^4}{\hat{s}^2} \{2(\hat{t} - m_i^2 - m_b^2)^2 + 2(\hat{u} - m_i^2 - m_b^2)^2 + (m_i^2 + m_b^2)\hat{s}\}, \quad (\text{B.2})$$

where $\hat{t} = (p_1 - b)^2$, $\hat{u} = (p_1 - \bar{b})^2$, and $p_1^2 = p_2^2 = m_i^2$.

B.2 Gluon fusion

Gluon fusion will also lead to $b\bar{b}$ (or $t\bar{t}$) jets. There are three diagrams contributing, including the one due to the three-gluon vertex ($p_1 + p_2 = p = b + \bar{b}$):

$$\begin{aligned} M &= M_1 + M_2 + M_3, \\ M_1 &= \bar{u}(b)ig\not{e}_1 T_a \frac{i(\not{b} - \not{p}_1 + m_b)}{(b - p_1)^2 - m_b^2} ig\not{e}_2 T_b v(\bar{b}), \\ M_2 &= \bar{u}(b)ig\not{e}_2 T_b \frac{i(\not{b} - \not{p}_2 + m_b)}{(b - p_2)^2 - m_b^2} ig\not{e}_1 T_a v(\bar{b}), \\ M_3 &= \bar{u}(b)ig\gamma_\mu T_c v(\bar{b}) \frac{g^{\mu\nu} - \xi p^\mu p^\nu / p^2}{p^2 + i\epsilon} \\ &\quad \times (-ig)f^{abc}[g_{\alpha\beta}(p_1 - p_2)_\nu + g_{\beta\nu}(p_2 + p)_\alpha - g_{\nu\alpha}(p + p_1)_\beta] \epsilon_1^\alpha \epsilon_2^\beta. \end{aligned} \quad (\text{B.3})$$

Since the final-state quark and antiquark are taken to be on-shell, the gauge-dependent part of M_3 vanishes. Properly averaged over spin and colour, the squared matrix element takes the form

$$\overline{|M|^2} = \frac{g^4}{2} [X + Y + Z], \quad (\text{B.4})$$

where X is due to M_1 and M_2 , Y is due to their interference with M_3 , and Z represents M_3 squared. Furthermore,

$$X = \frac{1}{(\hat{t} - m_b^2)^2} X_{tt} + \frac{1}{(\hat{t} - m_b^2)(\hat{u} - m_b^2)} X_{tu} + \frac{1}{(\hat{u} - m_b^2)^2} X_{uu}, \quad (\text{B.5})$$

with

$$\begin{aligned} X_{tt} &= \frac{8}{3} [(\hat{t} + m_b^2)(\hat{u} - m_b^2) + 2m_b^2(\hat{s} + 2m_b^2)], \\ X_{tu} &= -\frac{2}{3} m_b^2(\hat{s} - 4m_b^2), \\ X_{uu} &= \frac{8}{3} [(\hat{t} - m_b^2)(\hat{u} + m_b^2) + 2m_b^2(\hat{s} + 2m_b^2)]. \end{aligned} \quad (\text{B.6})$$

Similarly,

$$Y = Y_t + Y_u, \quad (\text{B.7})$$

with

$$\begin{aligned} Y_t &= \frac{-6}{\hat{s}(\hat{t} - m_b^2)} [(\hat{t} - m_b^2)^2 + \hat{s}m_b^2], \\ Y_u &= Y_t(\hat{t} \leftrightarrow \hat{u}) \end{aligned} \quad (\text{B.8})$$

and finally

$$Z = \frac{12}{\hat{s}^2} [(\hat{t} - m_b^2)(\hat{u} - m_b^2) - \hat{s}(\hat{s} + 2m_b^2)]. \quad (\text{B.9})$$

References

- [1] J. L. Hewett and T. G. Rizzo, Phys. Rep. **183**, 193 (1989).
- [2] P. Langacker and M. Luo, Phys. Rev. **D45**, 278 (1992);
P. Langacker, M. Luo and A. K. Mann, Rev. Mod. Phys. **64**, 87 (1992).
- [3] J. C. Pati and A. Salam, Phys. Rev. **D10**, 275 (1974); R. N. Mohapatra and J. C. Pati, Phys. Rev. **D11**, 566 (1975); G. Senjanovic and R. N. Mohapatra, Phys. Rev. **D12**, 1502 (1975); R. E. Marshak and R. N. Mohapatra, Phys. Lett. **91B**, 222 (1980).
- [4] A. Djouadi, A. Leike, T. Riemann, D. Schaile and C. Verzegnassi, Z. Phys. **C56**, 289 (1992);
A.A. Pankov and N. Paver, Phys. Rev. **D48**, 63 (1993);
S. Godfrey, 1996 DPF/DPB Summer Study on New Directions for High-Energy Physics (Snowmass, 1996), OCIP-C-96-6, hep-ph/9612384;
A. Leike and S. Riemann, Z. Phys. **C75**, 341 (1997);
A. Leike, Phys. Lett. **B396**, 245 (1997);
P. Osland and A. A. Pankov, Phys. Lett. **B403**, 93 (1997) and **B406**, 328 (1997).
- [5] F. Del Aguila and M. Cvetič, Phys. Rev. **D50**, 3158 (1994);
F. Del Aguila, M. Cvetič and P. Langacker, Phys. Rev. **D52**, 37 (1995);
M. Cvetič and S. Godfrey, Summary of the Working Subgroup on Extra Gauge Bosons of the DPF long-range planning study, hep-ph/9504216; in Electro-weak Symmetry Breaking and Beyond the Standard Model, eds. T. Barklow, S. Dawson, H. Haber and J. Siegrist (World Scientific, Singapore, 1995);
F. Del Aguila, M. Masip and M. Perez-Victoria, Acta Phys. Polon. **B27**, 1469 (1996);
K. S. Babu, C. Kolda and J. March-Russell, IASSNS-HEP-97-114, Oct 1997, hep-ph/9710441.
- [6] See, for example: H. Georgi, E. E. Jenkins and E. H. Simmons, Phys. Rev. Lett. **62**, 2789 (1989), Erratum: *ibid.* **63**, 1540 (1989);
F. Caravaglios and G. G. Ross, Phys. Lett. **B346**, 159 (1995);
P. Chiappetta, J. Layssac, F.M. Renard and C. Verzegnassi, Phys. Rev. **D54**, 789 (1996);
G. Altarelli, N. Di Bartolomeo, F. Feruglio, R. Gatto and M. L. Mangano, Phys. Lett. **B375**, 292 (1996);
M. L. Mangano, G. Altarelli, N. Di Bartolomeo, F. Feruglio and R. Gatto, in Proceedings of the 28th International Conference on High-energy Physics (ICHEP '96), Warsaw, Poland, 1996, p. 1332.

- [7] V. Barger, K. Cheung and P. Langacker, Phys. Lett. **B381**, 226 (1996).
- [8] L.B. Okun, Mod. Phys. Lett. **A11**, 3041 (1996);
S.I. Blinnikov, A.D. Dolgov, L.B. Okun and M.B. Voloshin, Nucl. Phys. **B458**, 52 (1996).
- [9] I. T. Dyatlov, Sov. J. Nucl. Phys. **52**, 9 (1990); Phys. Rev. **D43**, 2999 (1991);
Yad. Fiz. **54**, 265 (1991); Phys. Rev. **D45**, 1636 (1992).
- [10] B. Holdom, Phys. Lett. **B339**, 114 (1994).
- [11] P. H. Frampton, M. B. Wise and B. D. Wright, Phys. Rev. **D54**, 5820 (1996).
- [12] D. J. Muller and S. Nandi, Phys. Lett. **B383**, 345 (1996).
- [13] Physics at LEP2, Proceedings of the Workshop, Geneva, Switzerland (1996),
CERN 96-01, G. Altarelli, T. Sjöstrand and F. Zwirner, eds.
- [14] S. Kuhlman et al., (The NLC Accelerator Design Group and the NLC
Physics Working Group) *Physics and Technology of the Next Linear Col-
lider*: A Report Submitted to Snowmass '96 by the NLC Zeroth-Order De-
sign Group and the NLC Physics Working Group, BNL 52-502, FERMILAB-
PUB-96/112, LBNL-PUB-5425, SLAC-Report-485, UCRL-ID-124160, UC-
414, hep-ex/9605011;
ECFA/DESY LC Physics Working Group (E. Accomando et al.,), DESY-
97-100, Phys. Rep., to appear, hep-ph/9705442.
- [15] G. Altarelli, R. Casalbuoni, D. Dominici, F. Feruglio and R. Gatto, Nucl.
Phys. **B342**, 15 (1990).
- [16] D. Schildknecht, Talk given at International School of Subnuclear Physics:
34th Course: *Effective Theories and Fundamental Interactions*, Erice, Italy,
July 1996, preprint BI-TP 96/49; hep-ph/9610366.
- [17] Particle Data Group (R.M. Barnett et al.), Phys. Rev. **D54**, 1 (1996).
- [18] A. Blondel, in Proceedings of the 28th International Conference on High-
energy Physics (ICHEP '96), Warsaw, Poland, 1996, p. 205.
- [19] M. Veltman, Nucl. Phys. **B123**, 89 (1977);
M. Chanowitz, M. A. Furman and I. Hinchliffe, Phys. Lett. **78B**, 285 (1978).
- [20] J.J. van der Bij and F. Hoogeveen, Nucl. Phys. **B 283**, 477 (1987);
A. Djouadi et al., KA-TP-8-1997, Oct 1997; hep-ph/9710438.
- [21] M. E. Peskin and D. V. Schroeder, *Introduction to Quantum Field Theory*
(Addison-Wesley, New York, 1995), pp. 759, 763.

- [22] G. Altarelli, R. Barbieri and F. Caravaglios, preprint CERN-TH/97-290, hep-ph/9712368.
- [23] D. C. Kennedy and B. W. Lynn, Nucl. Phys. **B322**, 1 (1989).
- [24] H. Plathow-Besch, PDFLIB (CERNLIB), version 4.17; Comput. Phys. Commun. **75**, 396 (1993).
- [25] M. Glück, E. Reya and A. Vogt, Z. Phys. **C48**, 471 (1990) and **C53**, 127 (1992); Phys. Lett. **306B**, 391 (1993).
- [26] F. Abe et al., CDF Collaboration, Phys. Rev. Lett. **77**, 438 (1996).
- [27] B. A. Kniehl and J. H. Kühn, Nucl. Phys. **B329**, 547 (1990).
- [28] D. J. Muller and S. Nandi, Phys. Lett. **B383**, 345 (1996).
- [29] A. Leike, Phys. Lett. **B396**, 245 (1997);
A. Leike, S. Riemann and T. Riemann, Phys. Lett. **B291**, 187 (1992).
- [30] The LEP Collaborations ALEPH, DELPHI, L3, OPAL, the LEP Electroweak Working Group and the SLD Heavy Flavor Group (D. Abbaneo et al.), CERN-PPE/97-154, 1997.
- [31] S. Riemann, FORTRAN program ZEFIT Version 4.2;
D. Bardin et al., preprint CERN-TH 6443/92.
- [32] P. A. Baikov et al., hep-ph/9701412; in: Proc. of X Workshop on High Energy Physics and Quantum Field Theory (QFTHEP-96), ed. by B. B. Levtchenko and V. I. Savrin, Moscow, 1996, p. 101.
- [33] D. Choudhury and J. Kalinowski, Nucl. Phys. **B491**, 129 (1997).
- [34] R. Delbourgo and A. Salam, Phys. Lett. **40 B**, 381 (1972);
T. Eguchi and P. G. O. Freund, Phys. Rev. **37**, 1251 (1976).
- [35] L. Alvarez-Gaumé and E. Witten, Nucl. Phys. **B234**, 269 (1984).

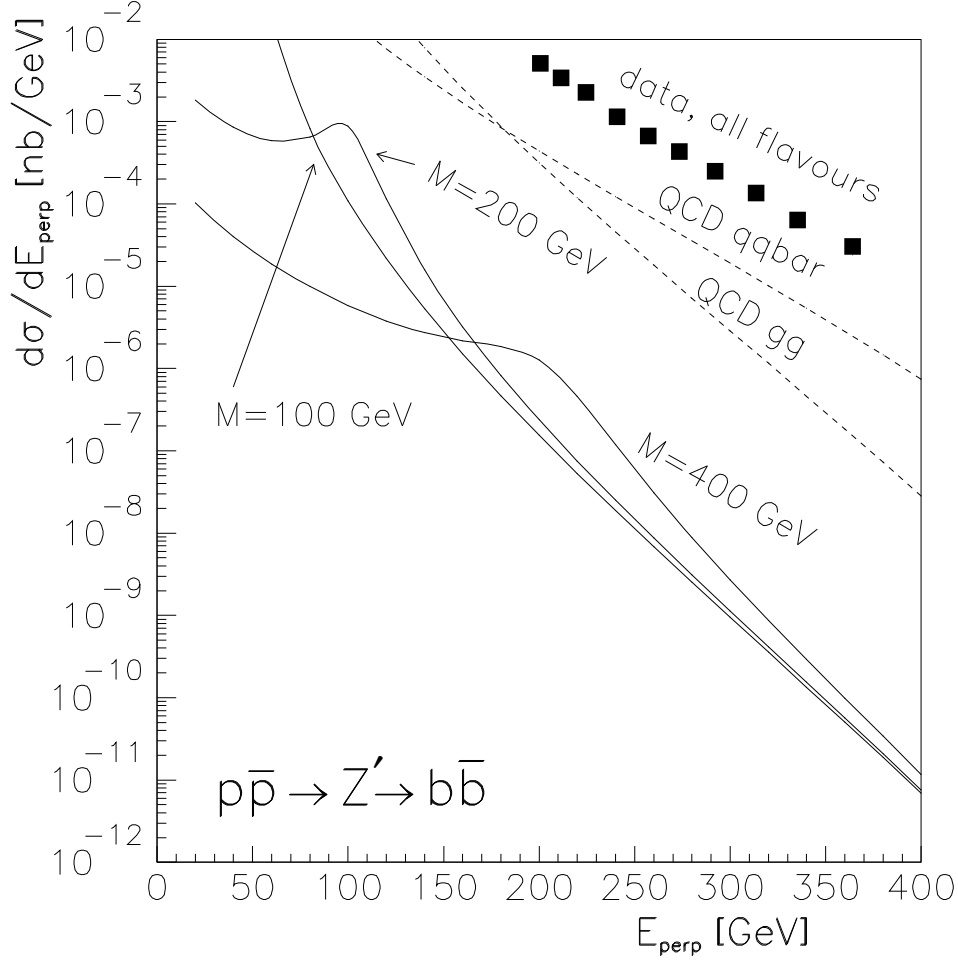


Figure 1. Cross sections for inclusive jet production at the Tevatron, $p\bar{p}$ collisions at $E_{\text{cm}} = 1.8$ TeV. The solid curves represent Drell–Yan-type production of Z' , from b and \bar{b} (sea) quarks in the initial state. Three masses are considered, $M_{Z'} = 100, 200$ and 400 GeV. The couplings are: $g_{Z'v'_b} = g_{Z'a'_b} = 1$. Also the contributions from the dominant QCD mechanisms are shown, as well as data (summed over all flavours) [26].

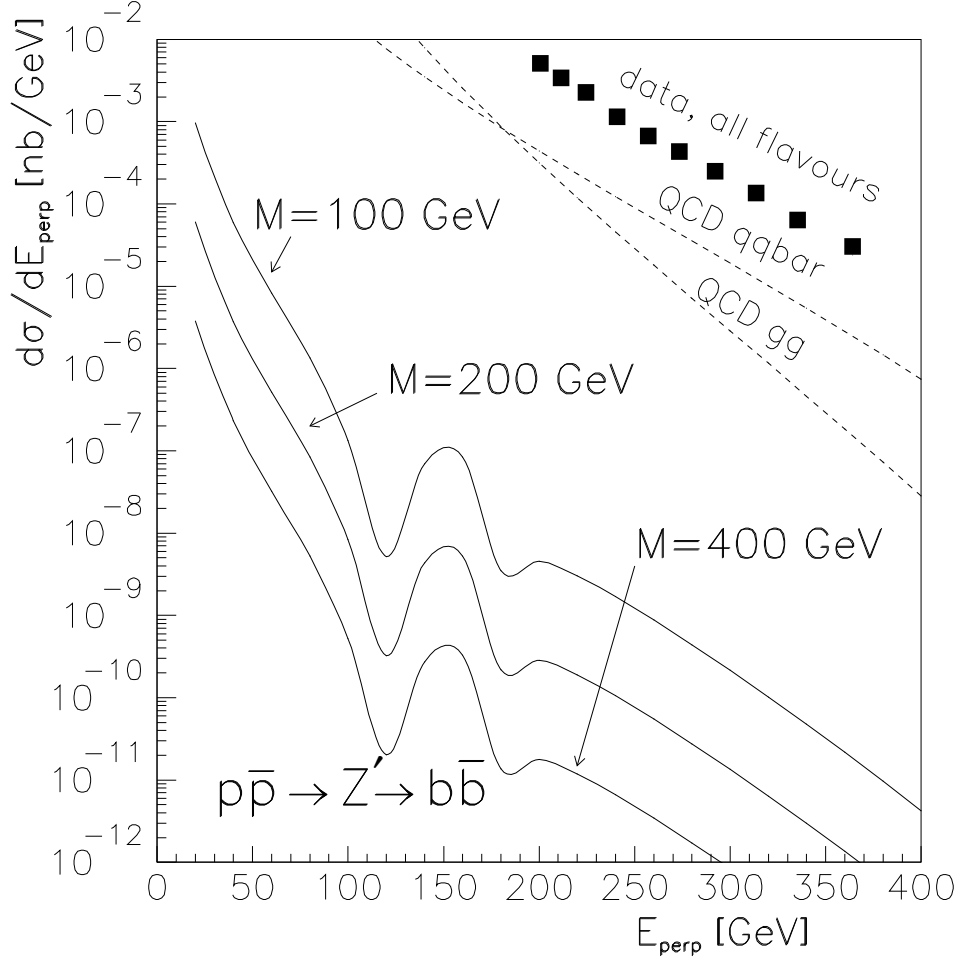


Figure 2. Cross sections for inclusive jet production at the Tevatron, $p\bar{p}$ collisions at $E_{\text{cm}} = 1.8$ TeV. The solid curves represent production of Z' , from gluon fusion. Three masses are considered, $M_{Z'} = 100, 200$ and 400 GeV. Both b and t quarks contribute to the triangle diagram, with equal couplings, $g_{Z'}a'_t = g_{Z'}a'_b = 1$. Also the contributions from the dominant QCD mechanisms are shown, as well as data (summed over all flavours) [26].

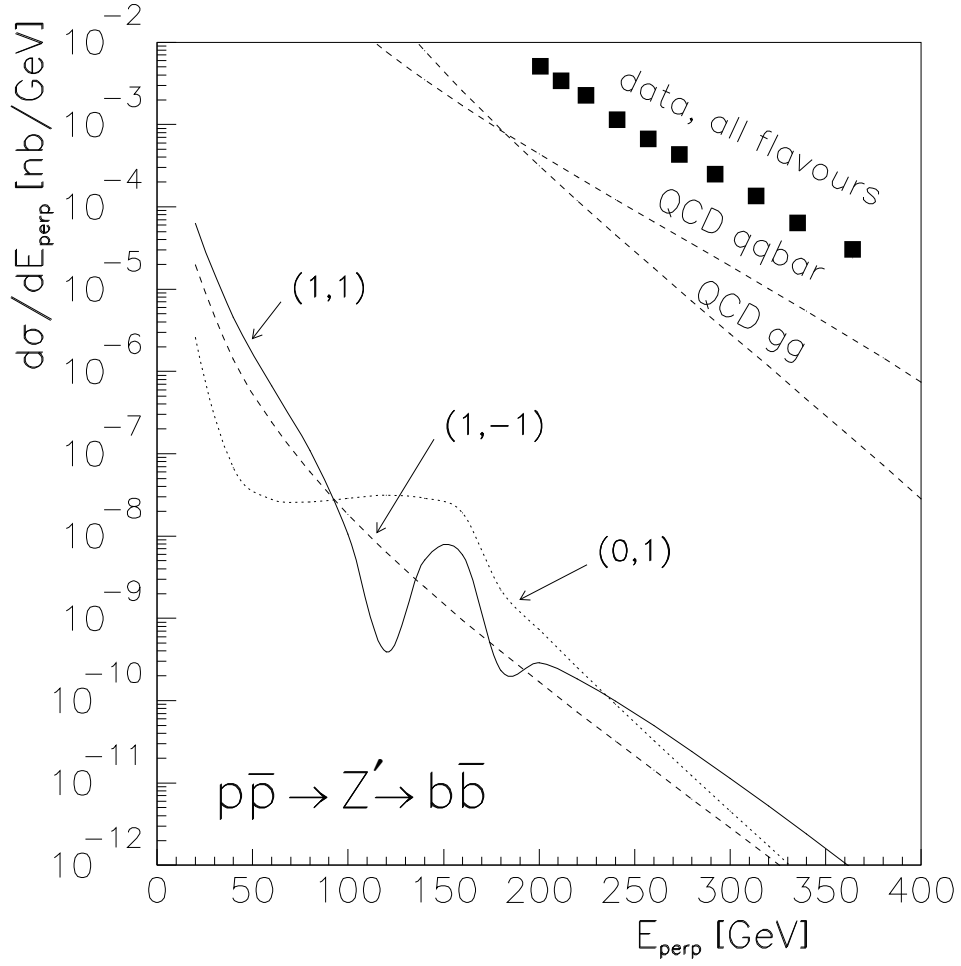


Figure 3. Similar to Fig. 1, but for $M_{Z'} = 200$ GeV only. Three cases of $q\bar{q}Z'$ couplings are considered: $(g_{Z'a'_t}, g_{Z'a'_b}) = (1, 1)$ (solid), $(0, 1)$ (dotted), and $(1, -1)$ (dashed).

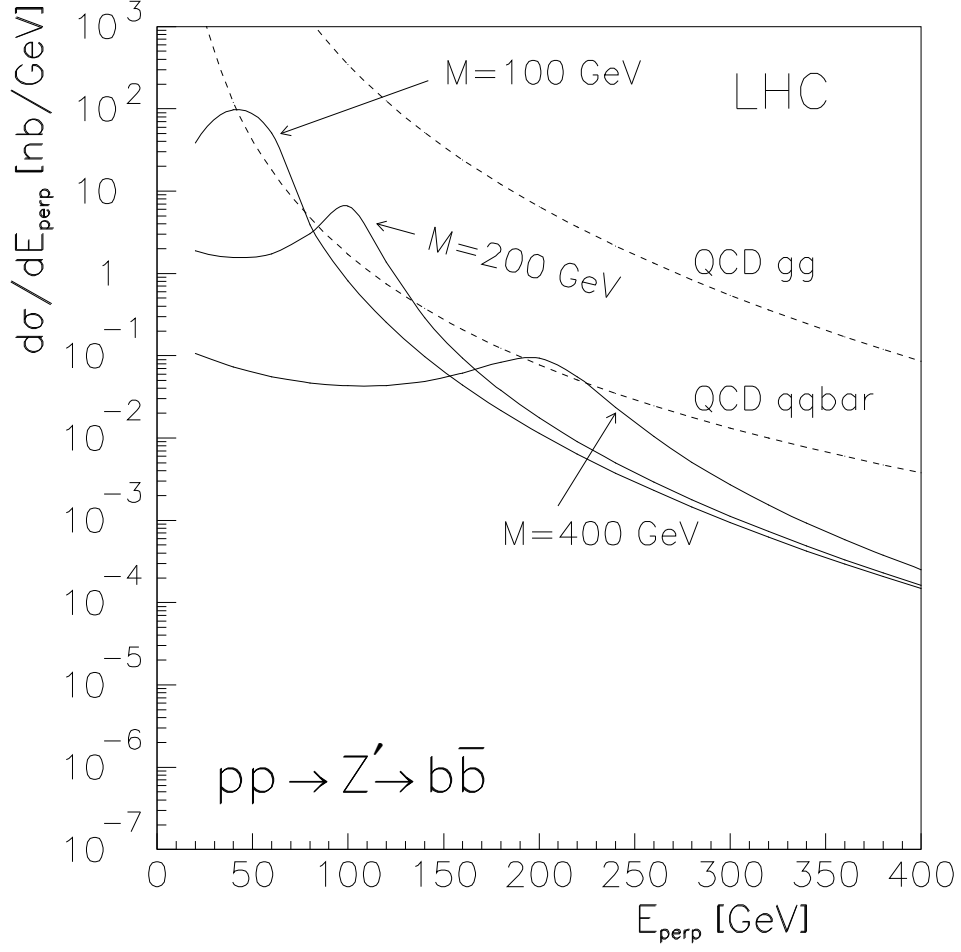


Figure 4. Cross sections for inclusive jet production at the LHC, pp collisions at $E_{\text{cm}} = 14$ TeV. The solid curves represent Drell-Yan-type production of Z' , from b and \bar{b} (sea) quarks in the initial state. Three masses are considered, $M_{Z'} = 100, 200$ and 400 GeV. Also the contributions from the dominant QCD mechanisms are shown, using standard distribution functions [24].

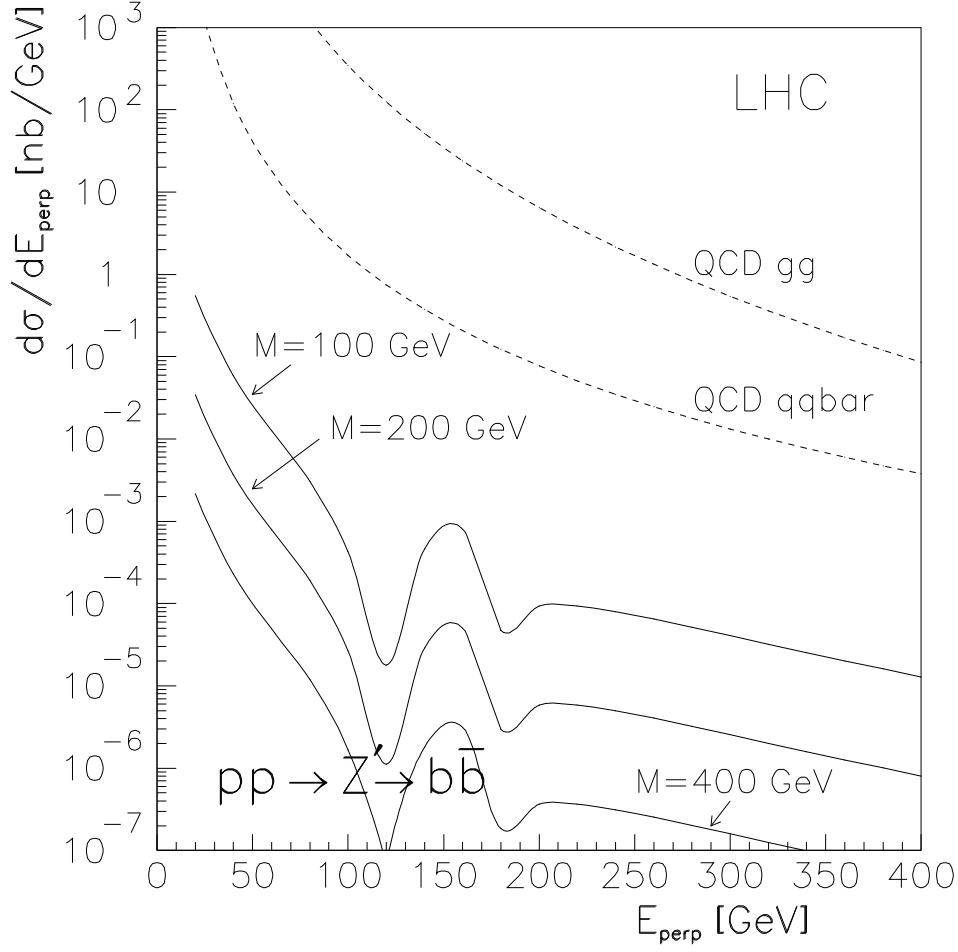


Figure 5. Cross sections for inclusive jet production at the LHC, pp collisions at $E_{\text{cm}} = 14$ TeV. The solid curves represent production of Z' , from gluon fusion. Three masses are considered, $M_{Z'} = 100, 200$ and 400 GeV. Both b and t quarks contribute to the triangle diagram, with equal couplings, $g_{Z'a'_t} = g_{Z'a'_b} = 1$. Also the contributions from the dominant QCD mechanisms are shown.

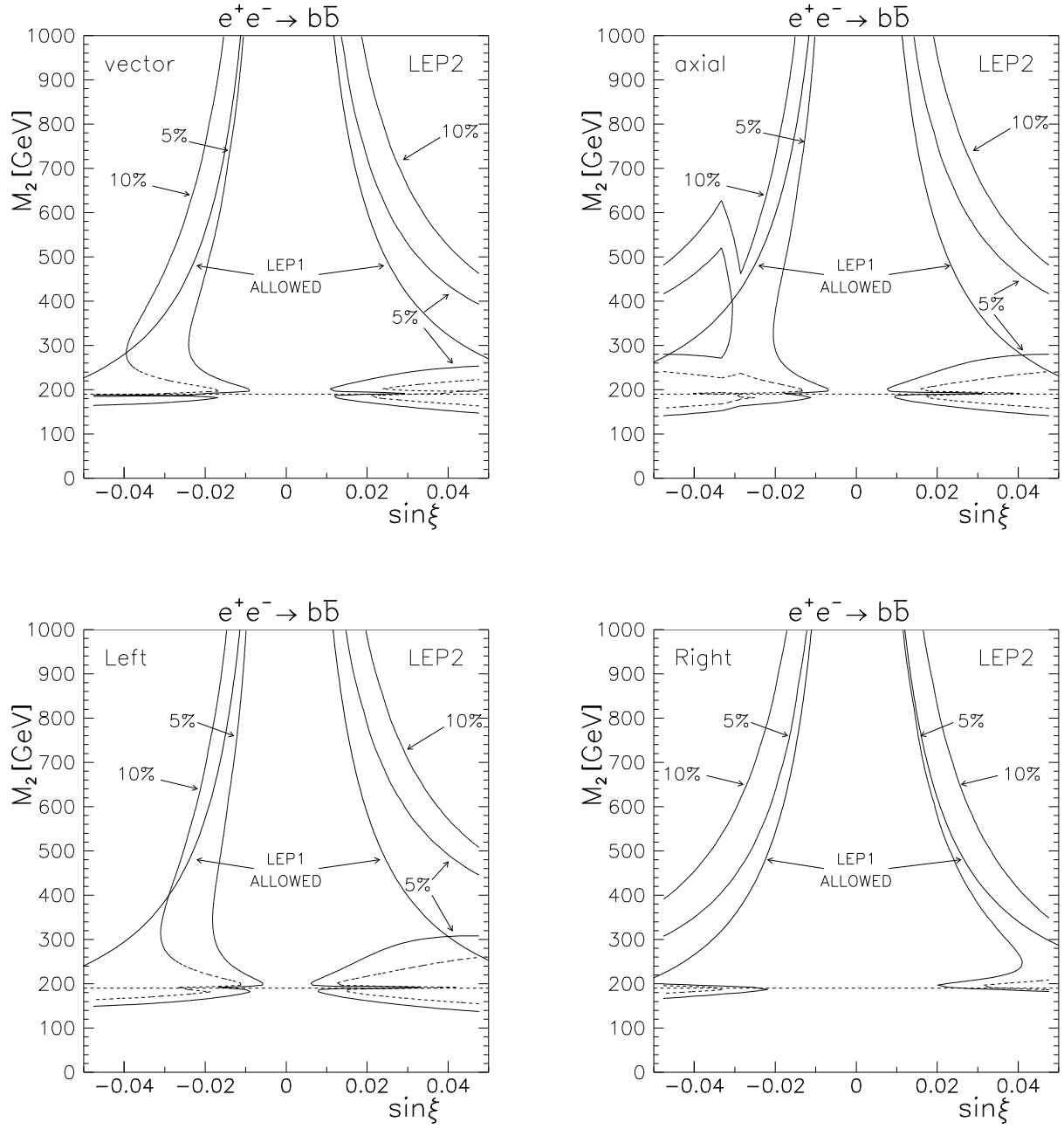


Figure 6. Allowed regions of $\sin \xi$ and M_2 obtained from LEP1 data (95% C.L.) for the process $e^+e^- \rightarrow b\bar{b}$. Also shown are bounds anticipated from LEP2 at levels of assumed precision as indicated by labels. Four different chiralities are considered.

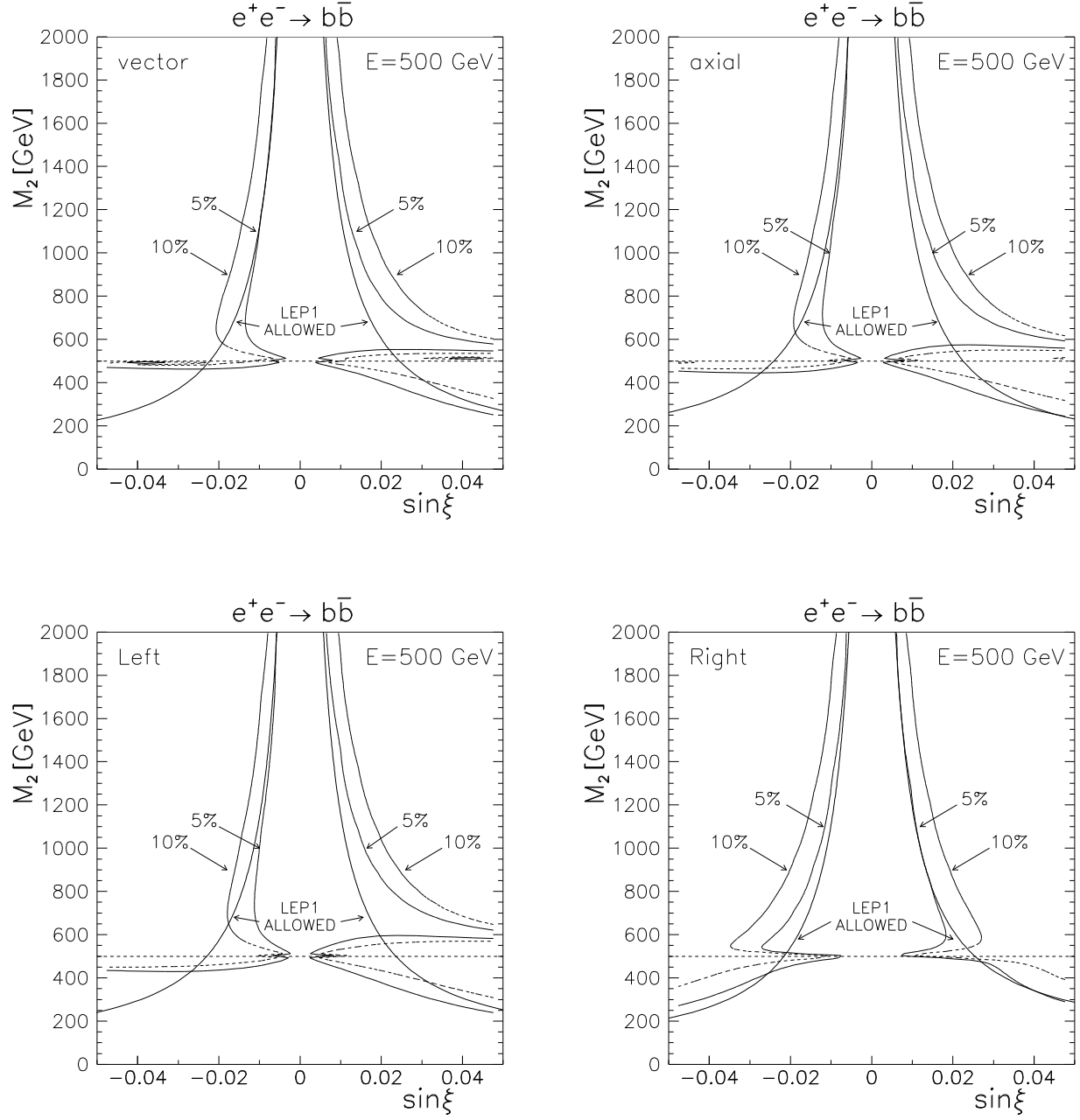


Figure 7. Allowed regions of $\sin \xi$ and M_2 obtained from LEP1 data (95% C.L.) for the process $e^+e^- \rightarrow b\bar{b}$. Also shown are bounds anticipated from 500 GeV at levels of assumed precision as indicated by labels.

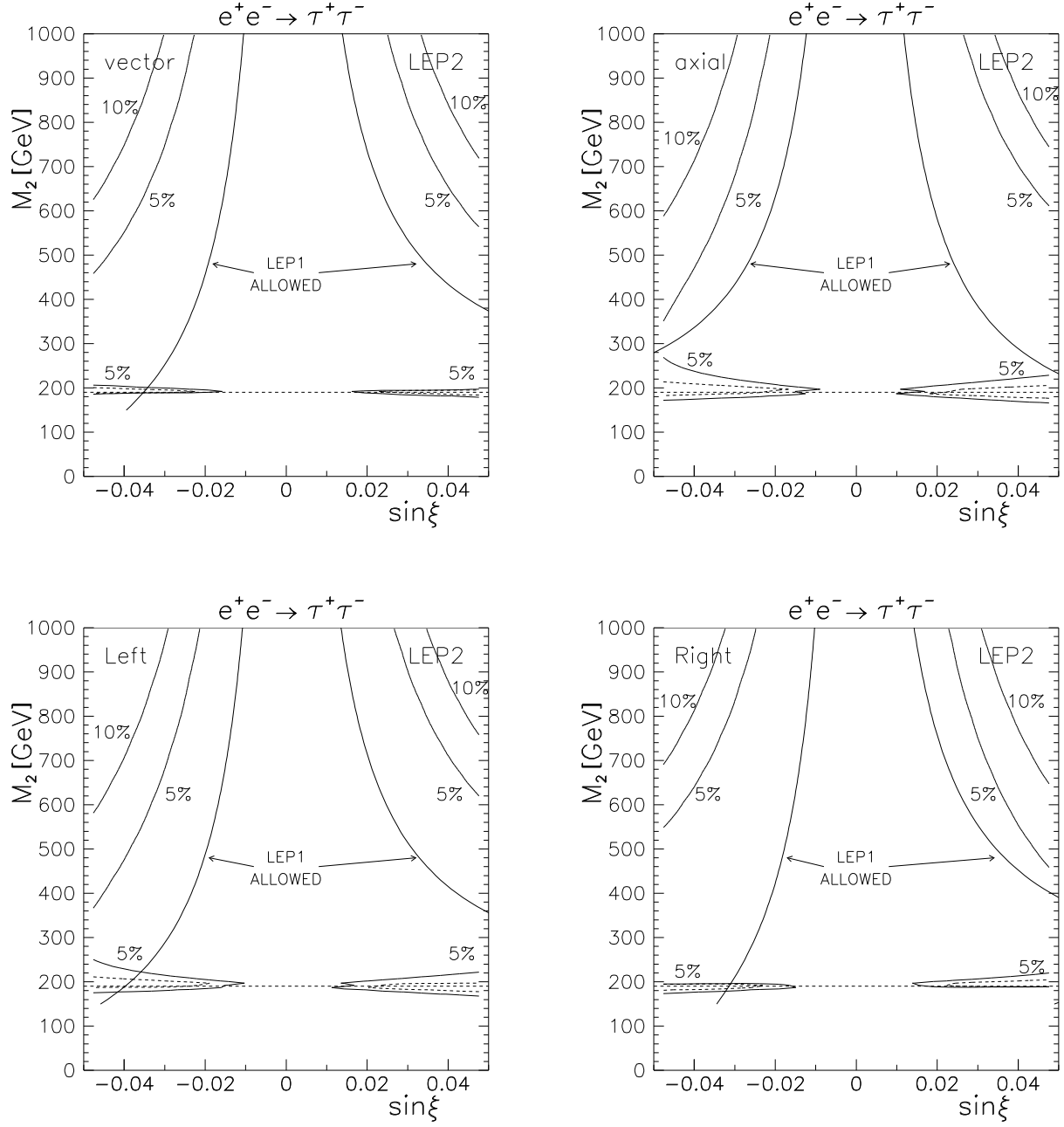


Figure 8. Allowed regions of $\sin \xi$ and M_2 obtained from LEP1 data (95% C.L.) for the process $e^+e^- \rightarrow \tau^+\tau^-$. Also shown are bounds anticipated from LEP2 at levels of assumed precision as indicated by labels. Four different chiralities are considered.

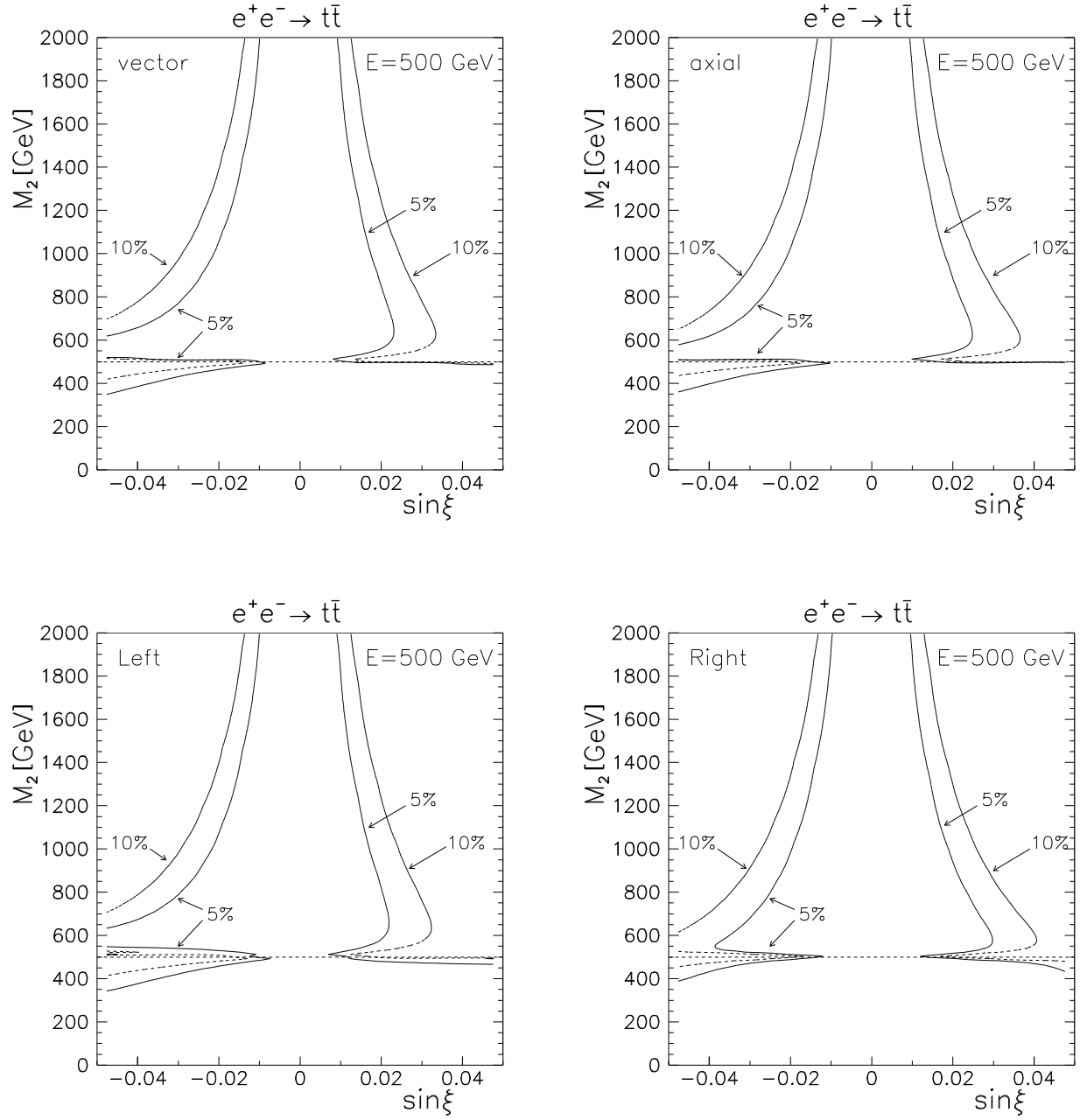


Figure 9. Allowed regions of $\sin \xi$ and M_2 anticipated for the process $e^+e^- \rightarrow t\bar{t}$ at the NLC at levels of assumed precision as indicated by labels. Four different chiralities are considered.

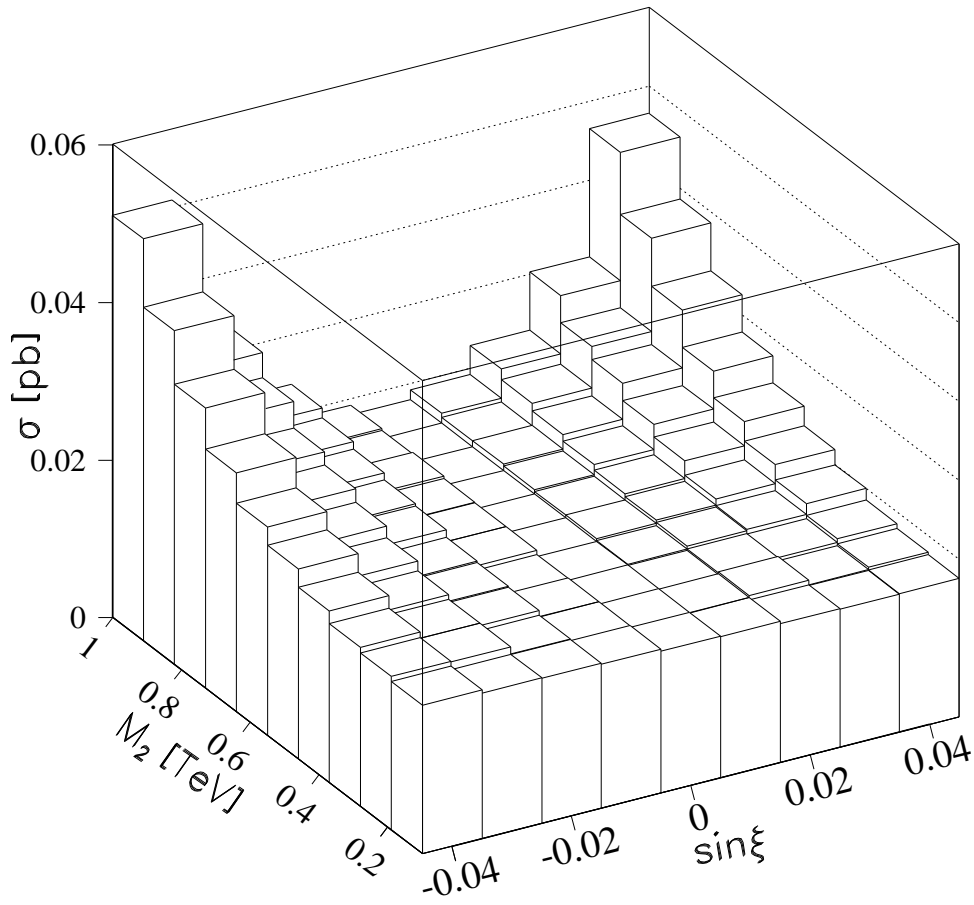


Figure 10. Cross section for $b\bar{b}\nu_e\bar{\nu}_e$ production at $\sqrt{s} = 190$ GeV, subject to cuts given by Eq. (4.10).

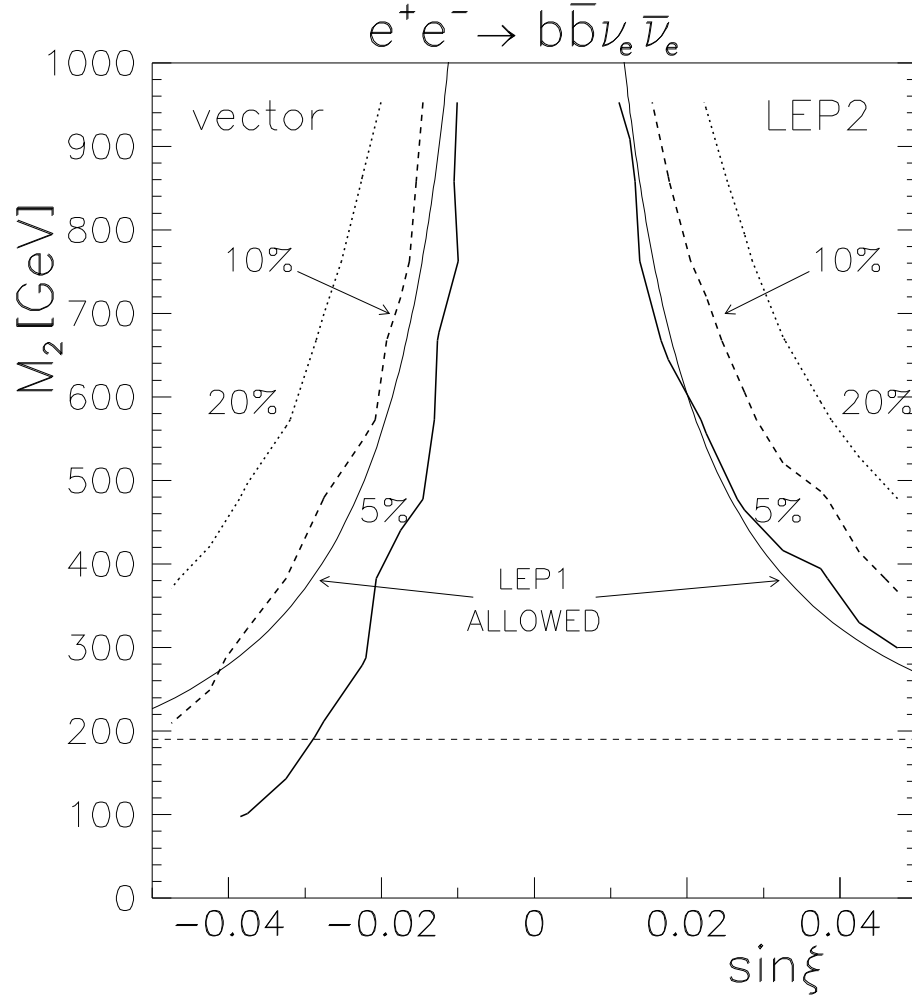


Figure 11. Bounds anticipated from LEP2 for $e^+e^- \rightarrow b\bar{b}\nu_e\bar{\nu}_e$ at levels of assumed precision as indicated by labels. Also shown is the allowed region of $\sin \xi$ and M_2 obtained from LEP1 data (95% C.L.) for the process $e^+e^- \rightarrow b\bar{b}$.

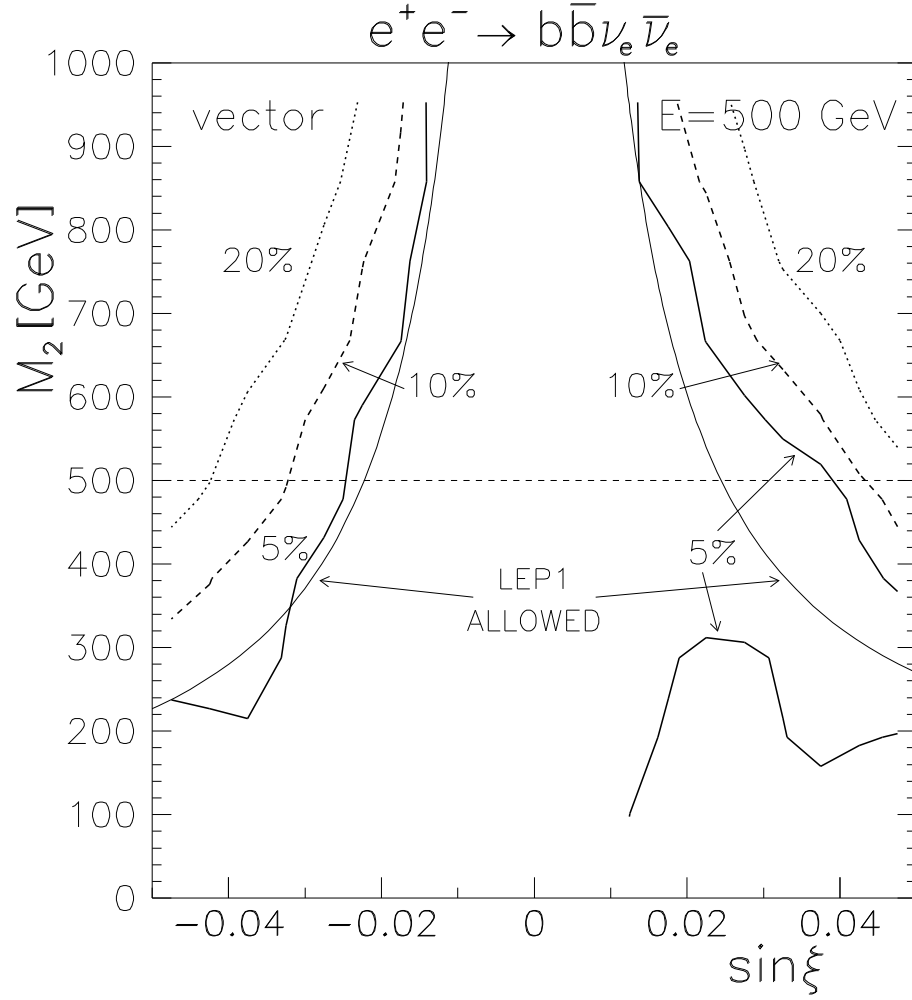


Figure 12. Bounds anticipated from $\sqrt{s} = 500$ GeV for $e^+e^- \rightarrow b\bar{b}\nu_e\bar{\nu}_e$ at levels of assumed precision as indicated by labels. Also shown is the allowed region of $\sin \xi$ and M_2 obtained from LEP1 data (95% C.L.) for the process $e^+e^- \rightarrow b\bar{b}$.